The atmospheric boundary layer over land and sea: Focus on the off-shore Southern Baltic and Southern North Sea region

Larsen, Søren Ejling

Publication date:
2013

Document Version
Publisher's PDF, also known as Version of record

THE ATMOSPHERIC BOUNDARY LAYER OVER LAND AND SEA: FOCUS ON THE OFF-SHORE SOUTHERN BALTIC AND SOUTHERN NORTH SEA REGION.

DTU Wind Energy
Department of Wind Energy

South Baltic PROGRAMME

This Project is part-financed by the South Baltic Programme and the European Union (European Regional Development Fund).

SOUTH BALTIC OFF.E.R

THE ATMOSPHERIC BOUNDARY LAYER OVER LAND AND SEA: FOCUS ON THE OFF-SHORE SOUTHERN BALTIC AND NORTH SEA REGION.

Søren E. Larsen
Danish Technical University
DTU WIN, Danish Technical University
Risø Campus, Roskilde, Denmark
E-mail: sola@dtu.dk

Abstract:

Lecture notes for a short course on the ideal atmospheric boundary layer and its characteristics for different types of real boundary layers, aiming at a discussion of the coastal conditions at the Southern Baltic and North Sea region.

The notes are aimed at young scientists (e.g. PhD students) that study the physics of the atmospheric boundary layer with the purpose of applying this knowledge for remote sensing techniques within offshore wind energy

Content

SOUTH BALTIC OFF.E.R

The Atmospheric Boundary Layer over land and sea: Focus on the offshore Southern Baltic and Southern North Sea region.

Søren E. Larsen

DTU WIN, Danish Technical University

Risø Campus, Roskilde, Denmark

Abstract:

Lecture notes for a short course on the ideal atmospheric boundary layer and its characteristics for different types of real boundary layers, aiming at a discussion of the coastal conditions at the Southern Baltic and North Sea regions.

The notes are aimed at young scientists (e.g. PhD students) that study the physics of the atmospheric boundary layer with the purpose of applying this knowledge for remote sensing techniques within offshore wind energy

Content

1 Introduction

The atmospheric boundary layer, ABL, is the lower part of the atmosphere, where the atmospheric variables change from their free atmosphere characteristics to the surface values. This means that wind speed goes from the free wind aloft to zero at the ground, while scalars, like temperature and humidity approach their surface value. An illustration of the profiles is shown on Figure 1.

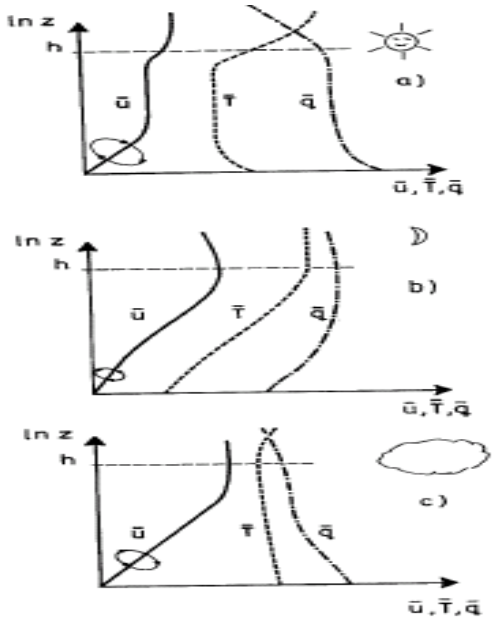

Figure 1. Profiles of mean speed, temperature and humidity (u, T and q) for a clear day, and night and cloudy conditions. Above the ABL height, h, we have the free atmosphere, while the ABL is below h down to the surface. Humidity is specified by its mixing ration q, being the ratio between the water and air density.

Characteristics of the atmospheric boundary layer, ABL, are of direct importance for much human activity and well being, because humans basically live within the ABL, and most of our activities take place here. The importance stems as well from the atmospheric energy and water cycles because the fluxes of momentum, heat, and water vapour between the atmosphere and the surfaces of the earth all pass through the ABL, being carried and modified by mixing processes here. Since these mixing processes mostly owe their efficiency to the mechanisms of boundary layer turbulence, a proper quantitative description of the turbulence processes becomes essential for a satisfying description of the fluxes and the associated profiles between the surfaces and the atmosphere.

Description of the structure of the flow, relevant scalar fields, turbulence and flux through the atmospheric boundary layers necessitates that almost all types of the flows, that occur there, must be considered. For these objectives, there are very few combinations of characteristic boundary layer conditions that are not of significant importance, at least for some parts of the globe.

2 Amospheric Boundary Layer (ABL) Flows.

The flow and other variables in the ABL all varies with space and time, and, neglecting the kinetic gas theory, its variability is characterised by a huge variation of the space and time scales that is involved. The larger spatial scales are related to the size of the globe, the weather systems and the depth of the atmosphere, the smaller scales are in the millimetre range. The time scales range between climate variation and milliseconds. The small scale limits are determined by the fluid properties of the atmosphere.

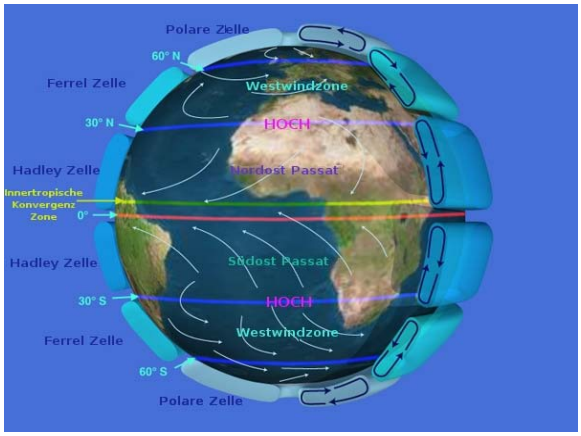

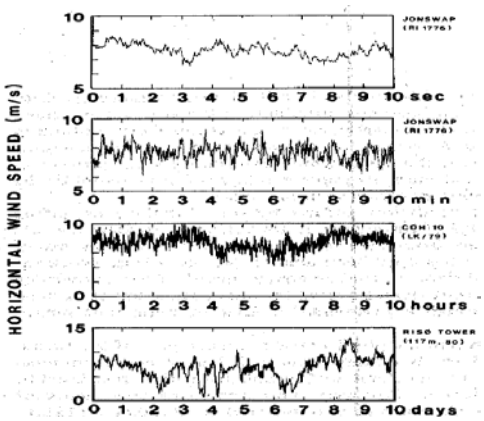

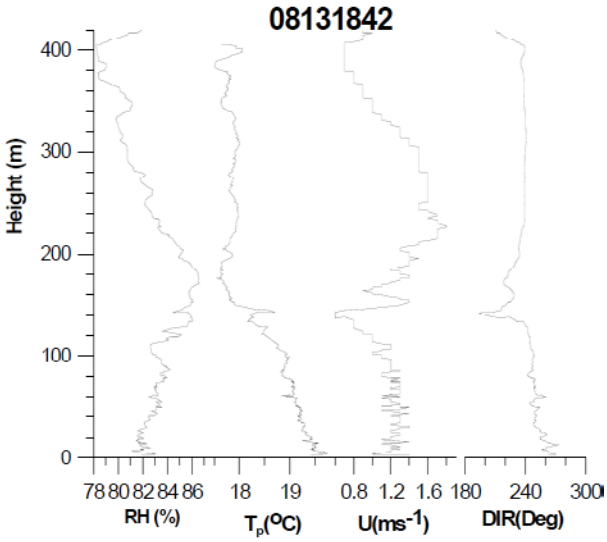

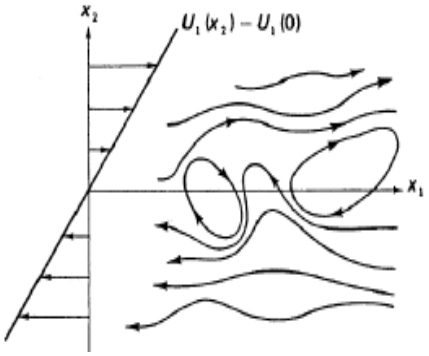

Figure 2. Large spatial scale variability for atmospheric flow at upper left, multiple temporal scale variability at upper right, and vertical multiple spatial scale Tethersonde data at lower left. A common name for the much of flow fluctuations in meteorology and fluid dynamics is turbulence, a term that further implies that at least part of its analysis and description is statistical. Production of turbulence from mean shear is illustrated at lower right (Tennekes and Lumley, 1972).

Important processes for ABL produced turbulence is the production of variability from the average velocity shear that has to exist in the ABL, as illustrated in Figure 1, because a fluid like the atmosphere gases cannot be dynamical stable with a mean shear as shown in Figure 1, and will start producing swirling motion, called eddies, see Figure 2. The characteristic spatial scales are the height where it happens, and/or the boundary layer height h. The thus created variability is called boundary layer turbulence, and is essential for the ABL mixing processes mentioned in the introduction.

For the purpose of mathematical treatment, one separates the variable in mean values and fluctuations like:

For velocity components: $u_i = \langle u_i \rangle + u_i'$, $\langle u_i \rangle$ in a mean value, u_i' is fluctuating turbulence, i =1,2,3

For scalars, T, and q, Temperature and humidity: $T = \langle T \rangle + T'$. $q = \langle q \rangle + q'$

Variances: $\langle u_i'^2 \rangle$, $\langle T'^2 \rangle$ also denoted by σ^2

co-variances and turbulent transport: $\langle u_i' u_j' \rangle$: Transport of u_i in the j direction (and vice versa).

$\langle u_i T' \rangle$, and $\langle u_i q' \rangle$:Transport of temperature and water vapour in the u_i direction. Multiplying the velocity co-variances by the air density, ρ , we can say that the velocity transport can be considered a momentum transport, similarly multiplying the temperature transport by ρC_p is converted to a heat transport, and multiplying the water vapour transport by ρL is converted to transport of latent heat Here Cp is the heat capacity of the air at constant pressure, L is the Heat of evaporation for water. Indeed these terms are often used in the description, since they reflect the physical importance better than the statistical term correlation.

Alternatively <> can be denoted with capital letters or overbars. The coordinate system can be described at x_i , i= 1,2,3 or with x,y,z , with the corresponding u_i or u,v,w, where u now is along the mean wind direction, w is vertical and v lateral (the second horizontal component).

A typical behavior of 600 seconds of ABL velocity components and temperature are shown on Figure 3.

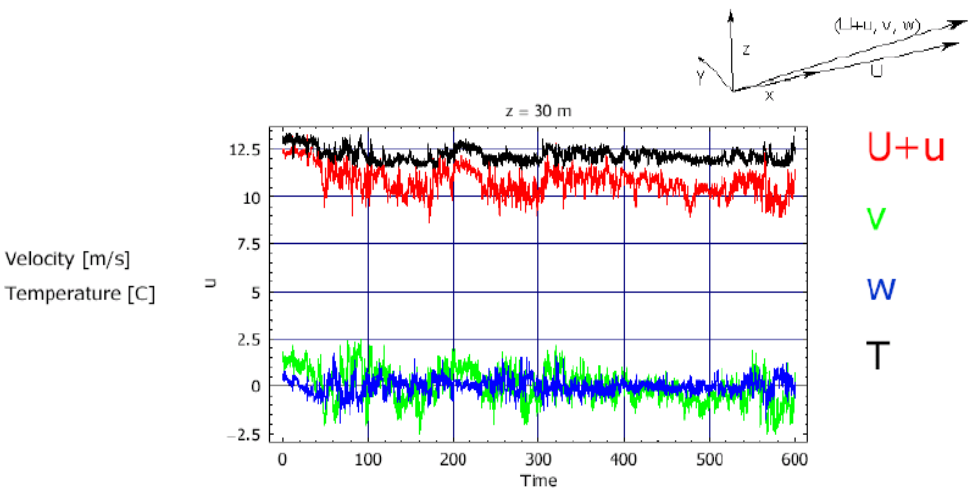

Figure 3: A 600 second record ABL mean values and turbulence: U+u', V+v',W+w' , and of T+T'. Notice, the coordinate system has a vertical z-axis and that the x axis is horizontal along the direction of the mean flow, meaning that V=0. The mean velocity is horizontal, because the mean vertical velocity, W∼0, since w is constrained by the nearby surface.

3 The ideal ABL.

As the simplest useful ABL, we assume the ABL to be limitted between a homogenous flat surface and a homogeneous boundary layer height,h, see figure 4.

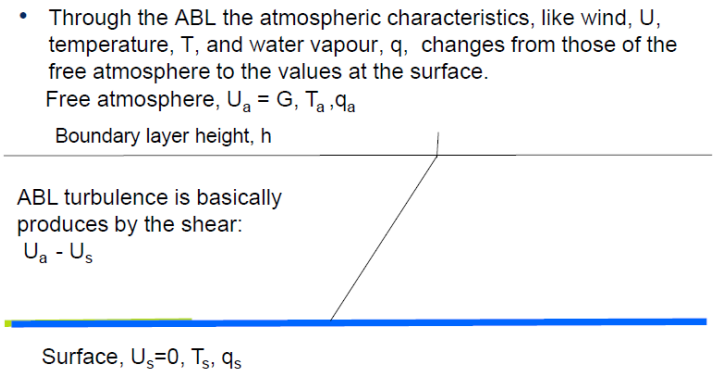

Figure 4. The ideal simplest atospheric boundary layer, ABL, which still provides realistic results. The conditions are statistically staionary and horizontally homogeneous. The wind speed is forced to zero at the surface,and attain the free wind value U_a in the free atmospheres above the ABL height,h. The values of wind , temperature and humidity are constant at the surface and above h, giving rise to a vertical flux of momentum, heat and water vapour between the surface and the h-level.

The flow is assumed statistically stationary, meaning there will be variations, but they will be statistically horizontally homogenous and stationary. However, as seen from equation (1) we must allow a pressure gradient that, again somewhat unrealistic, is taken as constant, because without pressure gradient, there will be no wind.

The three momentum equations.

$$\frac{D\overline{u_1}}{Dt} = 0 = -\frac{1}{\overline{\rho}}\frac{\partial \overline{p}}{\partial x_1} + f\,\overline{u}_2 - \frac{\partial}{\partial x_3}(\overline{u_1' u_3'})$$

$$\frac{D\overline{u_2}}{Dt} = 0 = -\frac{1}{\overline{\rho}}\frac{\partial \overline{p}}{\partial x_2} - f\,\overline{u}_1 + \frac{\partial}{\partial x_3}(-\overline{u_2' u_3'}).$$

$$\frac{D\overline{u_3}}{Dt} = 0 = -g - \frac{1}{\overline{\rho}}\frac{\partial \overline{p}}{\partial x_3} - 2\Omega(\eta_1\overline{u}_2 - \eta_2\overline{u}_1) - \frac{\partial}{\partial x_3}\overline{u_3' u_3'}.$$

The scalar equations:

$$\frac{D\overline{T}}{Dt} = 0 = \frac{\partial}{\partial x_3}(-\overline{u_3'\theta'})\ (= \frac{\partial T}{\partial t} + \overline{u}_1\frac{\partial T}{\partial x_1} + \overline{u}_2\frac{\partial T}{\partial x_2})$$

$$\frac{D\overline{q}}{Dt} = 0 = \frac{\partial}{\partial x_3}(-\overline{u_3' q'});$$

(1)

Equation (1) summarises the equation for the mean flow for our pseudo homogenous ABL. As mentioned the constant pressure gradient is necessary, but limits the horizontal scale for the model. The temperature equation further illustrates the meaning of the substantial derivative, for all the variables. The equation for u_3 is not important in this approximation and will be neglected in the following.

Additionally, in (1) our simplified ABL is situated on the rotating planet Earth, reflected by appearance of the Coriolis parameter, and the Earth´ rotation rate, Ω, with f =2 Ωsinφ, with φ being the latitude on the globe.

Further it is seen that we have introduced the symbol θ, the so called potential temperature that is a modified temperature including the fact that the average pressure and density in the atmosphere decreases with height, due to gravity. This means that an adiabatically moving air packet cools moving up and heats moving down, but will remain in equilibrium with surroundings and at the same potential temperature. If θ increases with height the air is denser than equilibrium at the bottom and therefore stable against vertical perturbations, and conversely for θ decreasing with height, the air is lighter than equilibrium at the bottom and hence unstable, if perturbed vertically. Within the boundary layer, θ is often approximated by:

$$\theta = T + \Gamma \cdot z, with\, \Gamma = g / C_p \qquad (2)$$

With Γ being about 0.01 K/m. It is noted that within the ABL, the only difference between T and θ is the linear height variation. For larger height variations, it is more complicated

Equation (1) shows that the vertical fluxes of scalars are constant with height, while the momentum fluxes are slightly more complicated. Focusing on the two first equations for the horizontal velocity components, we define the Geostrophic wind, G, from the pressure gradient, and perpendicular to the direction of this gradient:

$$G = (U_{1G}, U_{2G}) = (-\frac{1}{f\,\overline{\rho}}\frac{\partial \overline{p}}{\partial x_2}, \frac{1}{f\,\overline{\rho}}\frac{\partial \overline{p}}{\partial x_1}) = (-\frac{1}{f\,\overline{\rho}}\frac{\partial \overline{p}}{\partial y}, \frac{1}{f\,\overline{\rho}}\frac{\partial \overline{p}}{\partial x}); \qquad (3)$$

The two first equations in (1) now take the form:

$$\begin{aligned} 0 &= f\,(\overline{u}_2 - U_{2G}) - \frac{\partial}{\partial x_3}(\overline{u_1' u_3'}) \\ 0 &= -f\,(\overline{u}_1 - U_{1G}) - \frac{\partial}{\partial x_3}(\overline{u_2' u_3'}). \end{aligned} \qquad (4)$$

This equation shows that the wind velocity approach the Geostrophic wind at the top of the boundary layer, where the turbulence disappears. Down through the boundary layer the wind solution depends somewhat on the additional assumptions, but generally it depends on a balance between the pressure force, the Coriolis force that varies wind speed, the turbulence friction force varying with height and turbulence structure. As a result the wind undergoes a spiraling motion as it reduces to zero at the ground, see Figure 5.

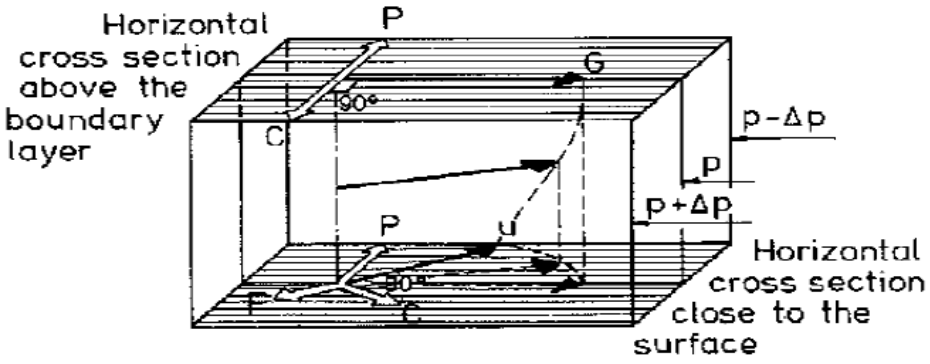

Figure 5. The variation of wind speed and wind direction from the top, through the ABL towards the ground. The wind profile can be seen as being developed through a balance between the three forces, the pressure gradient, P, the Coriolis force, C, and the Frictional force, F.(Larsen and Jensen, 1983)

The detailed behavior of the wind speed through the ABL is simplest for atmospheric neutral stability, meaning that there is no heat flux and water vapor flux between the surface and the free atmosphere in Figure 4. This can be assured by keeping the potential temperature, $\Delta\theta_h$, difference at zero, meaning that Ta-Ts =Γh, compare (2), and as well $q_s=q_a$.. For such situations one can derive the equations in (7), using so called scaling laws, where the momentum transport, considered above is a new scale introduced from the co-variance, the so called friction velocity u_* as :

$$u_*^2 = \overline{-u'w'} \tag{5}$$

$$ABL: \frac{\kappa G}{u_*} = \left((\ln(\frac{u_*}{fz_0}) - A)^2 + B^2 \right)^{\frac{1}{2}}$$

$$ABL: \alpha = \tan^{-1}(-B / (\ln(\frac{u_*}{fz_0}) - A)) \tag{6}$$

$$SBL: U(z) = \frac{u_*}{\kappa}\ln(\frac{z}{z_0})$$

The first equations relate the conditions at the top of the ABL to the wind at lower heights the so called Surface Boundary Layer, ASL. The first of these is called the resistance laws of the ABL, relating the friction velocity, u_*, to the Geostrophic wind, G, and a the so called roughness length, z0, plus three additional "universal" constants, the v Karman, κ , and the two constants A and B. The term $u*/fz_0$ is denoted the surface Rossby number. Since f is of the order of 10^{-4} s^{-1}, A is about 2 and B about 5, and z_0 is typically small, the Rossby number term dominates the first of the resistance laws. The second of the Resistance Laws estimates the angle between the Geostrophic wind the wind in the lower part of the ABL, the ASL. In this part the wind profile is described by the last of the equations, the so called Logarithmic Profile.

The set of equations allow us to estimate the wind profile in the ASL for a given Geostrophic wind speed for varying roughness length. Therefore the roughness length is a very important parameter, see Figure 7. In the principle it is a characteristic length, where the velocity extrapolates to its surface value, which is zero, but since it is a measure of the "roughness" of a given landscape, much effort has been aimed at establishing consensus about the roughness of characteristic real landscapes.

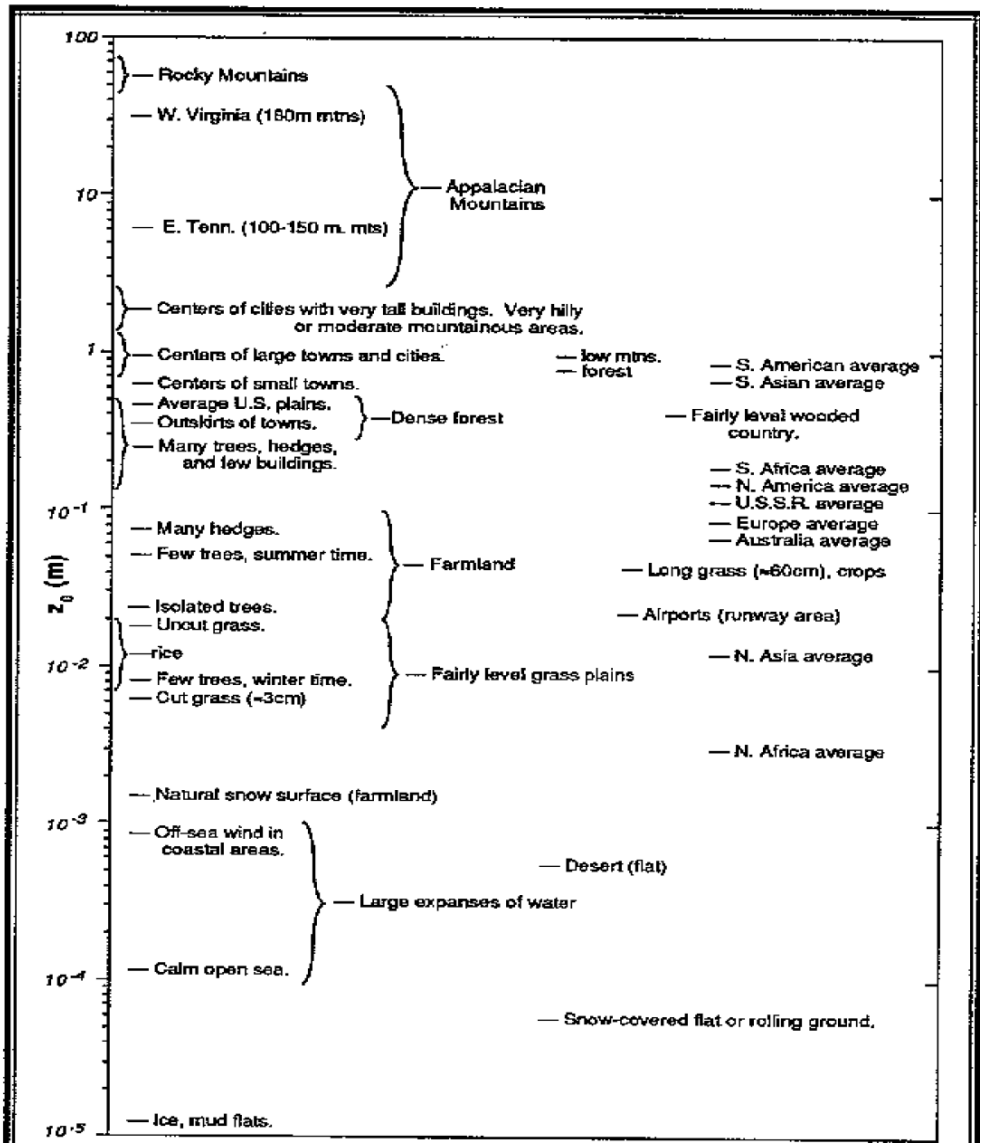

Figure 6. Consensus relations between the roughness lengths for different landscapes (Stull, 1988).

As seen from Figure 6, the roughness generally follows the intuitive images of what that roughness is associated with "roughness elements" protruding from the surface. The larger, sharper and within limits denser the protuding elemnts, the larger the roughness. Although this image is simplistic, it still summarise the main aspects of the roughness characteristics of landscaspes, including season variation of some landscapes.

To emphasize the imporance of the roughness length for wind energy, we compare in Figure 7 the winds in the ASL for for different roughness values and a given Geostrophic wind.

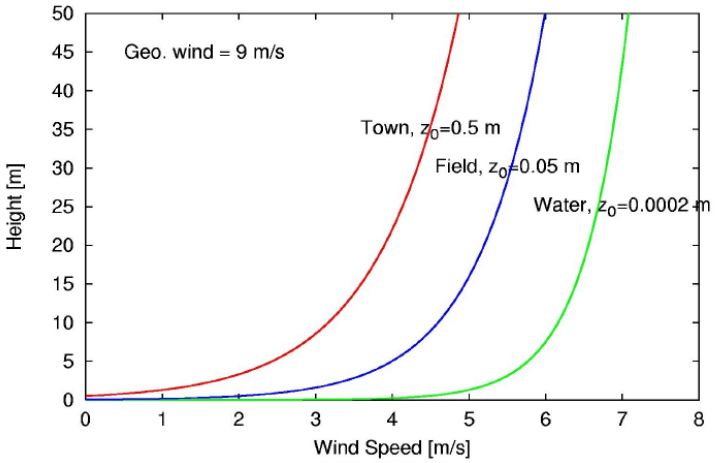

Figure 7. The change in surface wind for different roughness values, but the same Geostrophic wind, G. The roughness length z_0 is seen to be related to the indicated land scapes in Figure. 6

Until now we have considered only situations, where the potential temperature differences between the surface and the free atmosphere is unimportant for the dynamics, this state is called thermally neutral. Changing T_a and T_s to make $\Delta\theta_h$ different from zero, and similarly for q_s and q_a, a heat flux and water vapour flux must flow between the top of the ABL and the surface, and there will be a density gradient between top and bottom. For such a situations the variation of wind speed, temperature and humidity can be described by an extension of the simple scaling used for neutral conditions in (6). These scaling formulations are normally denoted the Monin-Obuchov formulation. The set of scales is summarised below, equation 7:

$$Friction\ velocity: u_* = -\overline{u'w'};\ Temperature\ scale: T_* = -\overline{w'\theta'}/u_*;$$

$$Water\ vapour\ scale: q_* = -\overline{w'q'}/u_*;\ Monin-Obuchov\ stability\ length: L = \frac{Tu_*^2}{\kappa g(T_* + 0.61q_*)} \quad (7)$$

The water vapour concentration, q, enters into the stability measure, because both q and θ influences the density and thereby the stability based on density fluctuations. This will be repeeted throughout this text, but not always, because temeperature is typically more important than humidity for the stability.

The Monin-Obuch scales are widely used not only in the atmospheric surface layer (ASL) that was introduced in Figure 5, but also for extension into the full ABL. In (7), g is the acceleration due to gravity, and the stability length, L, is a scale that is derived from the turbulence energy budget as a measure of the importance of the heat and water vapour fluxes relative to the momentum flux. As in (6) κ is the v. Karman constant.(~ 0.4). The scales defined in (7), change relatively little within the ASL, above this one typically uses the ASL measured parameters,

Corresponding to the neutral wind profile in (6), we can now formulate the set of stability influenced profiles in (8), as:

$$\overline{u}(z) = \frac{u_*}{k}\left(\ln\left(\frac{z}{z_0}\right) - \psi\left(\frac{z}{L}\right)\right)$$

$$\overline{\theta}(z) - \theta_0 = \frac{\theta_*}{k}\left(\ln\left(\frac{z}{z_{0T}}\right) - \psi_T\left(\frac{z}{L}\right)\right) \qquad (8)$$

$$\overline{q}(z) - q_0 = \frac{q_*}{k}\left(\ln\left(\frac{z}{z_{0q}}\right) - \psi_q\left(\frac{z}{L}\right)\right)$$

Stability influenced profiles of <u(z)>, <θ(z)> and <q(z)> . Notice, that separate "roughnes length" parameters are introduced for the scalars. These are of the order of z_o for smooth surfacaes, but typically of the order of 10 times less for rough surfaces.

From the definition of L, it is seen that z/L $\sim$0 for neutral conditons, with no scalar fluxes. $\psi(0) = 0$ for all three ψ-functions, and hence the logarithmic profiles for all variable are recovered for neutral. Close to the ground z/L $\sim$0 simply because z is close to zero. Hence all profiles start as being logarithmic close to the ground. For stable conditions, we have: $\psi(z/L) \sim -5/L$. For unstable conditions (meaning z/L<0) the functions are more complicated but can be approximated by is $\psi(z/L) \sim 1-(1-a\cdot z/L)^{-n}$, with a between 10 and 15, and n = 0.25 for the wind and 0.5 for the scalars.

When the heat flux is positive (the ground is warmer that the air) the atmosphere is characterised by rising air, the shear produced eddies are enhanced by the thermal structure, and the situation is denoted thermally unstable. If the heat flux is downward, the shear produced eddies and the general fluctuation level is diminished, for which reason the the situation is denoted stable. The enhance mixing for unstable condition reduces the wind shear, while the reduced fluctuation level for stable condition allows a larger wind shear. The situations are depicted in Figure 1, where stability is indicated by sun, moon and a cloud . Notice that above the ABL the temperature and the potential temperature will in general increase with height.

In reality thermal properties of the lowest atmosphere is forced either by the radation balance at the ground, insolation at day time, and radiational cooling at night time, or/and by advection of air mases with a temparature that differs from the surface temperature. The balance depends on time scale considered, on the thermal properties of the gound, cloud cover and the characteristics of the air motion around the site. We return to this when discussing real boundary layers.

As opposed to the profiles in (8), in engineering litterature one often find the socalled power law profiles for wind speed:

$$u(z)/u(z=10) = (z/10)^{\alpha}, \qquad (9)$$

where the relevant α will be function of height , stability and roughness, as seen by comparing with (8). The power law profile has the advantage of being simple and that α is a direct measure of the dimensionsless relative shear, as can be seen by differentiation of (9).

For neutral conditions we have in (6) not only a wind profile in the ASL, but also for the whole ABL a resistance law relating the G to u_* and the Geostrophic wind angle. This can in the principle be extended also to different stabilities and to the scalar variablse, letting the A and B constants, and corresponding parameters for scalars, be function of stablity, typically in terms of h/L. (Zillitinkevich, 1972,1975) However, the quality of the data fit for these extensions are worse than for the simple neutral expression in (6), and therefor they are not much used.

For our ideal boundary layer discussion, we have simply fixed the boundary layer height, just as we could fix the temperature difference between the surface and the air on the top of the ABL. In the real world the ABL height is determined as the outer range of the aboundary layer turbulence. For ideally neutral conditions it must be proportional to u_* /f, since these two parameters are the only parameters available to characterise the ABL turbulence. Indeed one finds that this fits the data moderatedly well with a coefficent euqual to about 0.3. For moderate stabilities, one can use expressions like $h \sim 0.7(u_* L/f)^{0.5}$, and for strongly stable conditions $h \sim L$, the Monin-Obuchov stabily length.

For unstable and many stable situations, it is common to use an independen rate equation, to determine h, at least over land, that h= h(t) is now derived from an equation like. $dh/dt \sim F(\cdot\cdot)$. Especialy for unstable situations, a very simple and successfull equation has been developed assuming an unstable ABL growing, in response to sunrise, against a background stable potential temperature gradient, γ, using the instationary temperature equation in (1). The result is

$$h(t) = \left(2\frac{Q(t)}{\gamma} \right)^{\frac{1}{2}} \quad \text{with } Q(t) = \int_0^t \overline{w'\theta'}\big|_0 (1+2A)dt' , \tag{10}$$

Where A here is an entrainment coefficient of the order of 0.2, accounting for the flux is not only from the ground, but also from the top of the growing ABL. The boundary layer height and the roughness length in combination have importance for the exsistence and extent of the surface boundary layer. Formally ASL can exist for $z_0 << z << h$. For the large z_0 in Figure 6 and low values of h, the simple ASL expression of (8) becomes invalid.

Note, that with equations like (10) , we have strickly speaking left the stationary boundary layer, and are approaching the real world, where a diurnal cycle is a basic fact of life. Experience shows, however that much of the simplified ABL described here survives, when allowing for slower changes like many, but not all, of the diurnal changes.

Not only mean values are important to characterise the ABL, also fluctuatuation of the individual signal are important. To a first approximation these can be chacterised by the turbulence standard deviation, where

especially those associated with the velocity components are important for many puposes. One has developed expressions, corresponding to the Monin-Obuchov profile expressions considered above:

$$\frac{\sigma_x}{X_*} \approx F(\frac{z}{L}, \frac{h}{L}) \; with \; X = u_i, \theta, or \; q \,, \tag{11}$$

Where it has been found necessary to include h/ L even within the ASL. In general the function F increase with increasing instability, and become constant for neutral-stable condition. For velocity one often considers (11) in term of the Turbulence Intensity (TI) derived from (11) by division with the local wind speed. Thereby the TI become an expression for the likely relative deviation from the mean speed one will encounder for given situations, Also distributions of the vertical instantaneous shear has become an important parameter, e.g. distributions of α in (9). Insering the respective expressions we get, for the two:

$$TI = \frac{\sigma_u}{\overline{u}} = \frac{\kappa F(z/L, h/L)}{\ln(z/z_0) - \psi(z/L)} \approx \frac{1}{\ln(z/z_0)} \; for \; \frac{z}{L} \to 0$$
$$\alpha = \frac{z}{\overline{u}} \frac{d\overline{u}}{dz} = \frac{\phi(z/L)}{\ln(z/z_0) - \psi(z/L)} \approx \frac{1}{\ln(z/z_0)} \; for \; \frac{z}{L} \to 0 \tag{12}$$

,

(12)

,

where φ(z/L) is the derivative of ψ(z/L). The bahviour of data on the two functions are shown i Figure7.

Additional information about the the fluctuations can be sought in the correlations or the spectral structure of the signals. Atmospheric signals vary as function of both time and space. For boundary layer turbulence, one can mostly assume that the fluctuations vary with space only, and that measured time variation at a stationary measuing station is due to advection of a spatial variation of the signal.

This, surprisingly simple assumption, is denoted the Taylor hypothesis. Take a measured u (t) as an example:

$$u(\Delta t) = u\,(\Delta x / \langle u \rangle) \tag{13}$$

where Δ signify that the Taylors Hypothes works on diffences in space and time, not on the absolute coordinates. Equation13 can even be used in connection with a moving sensor, like an air plane, where the speed then must be the sum of the air velocity and the sensor velocity.

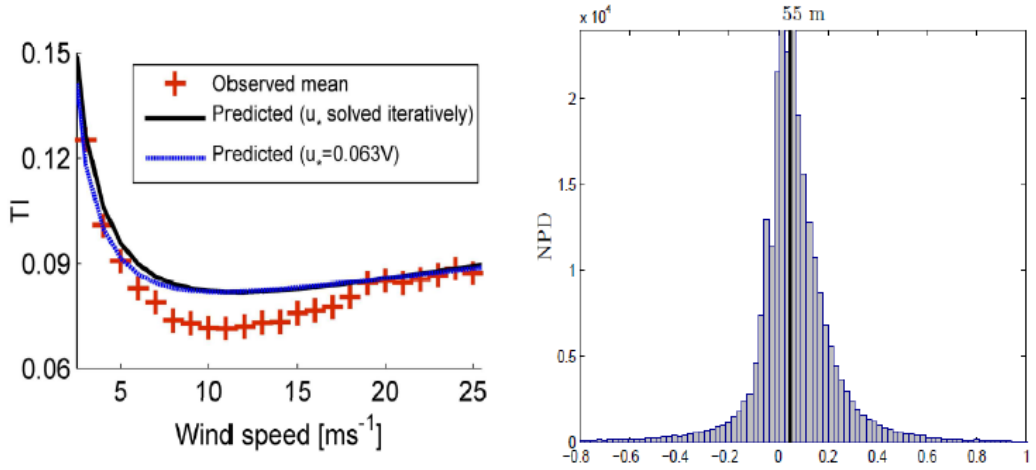

Figure 8 Behaviour of the Turbulent intensity the dimensionless shear from (12) , easured at about 60 meter over water (Wang et al, 2013, and Pena et al, 2012). The deviations between the predicted values and the data are due to stability, processes, and also to some extent to model failings, which we will comment later, but at the very least we see that the neutal limit with a constant z0 is not adequate to explan the data. Specifically for the TI it is fairly well established that the high TI for low wind speeds is due to stability effects. For higher winds TI is expected to folow the observed mean TI is expected to be in the neutral limit of (12). Hovever, the prediction is based on land conditions with a constant z_0, while the over water measurements, reflects the growth of z_0 with wind speed, following Charnock's relation as discussed in section 4.3.

To resolve frequency or wave number distribution of the turbulent variables, one uses Fourier spectra computed either as frequency or wave number spectra, with connection derived from the Taylors hy- pothesis, $\omega = k_1 \langle u \rangle$, where k_1 is the wave number along the mean wind direction . The Fourrier analysis is based on the existence of Fourrier pairs. The simplest principal way is to illustrate the spectra-correlation duality by:

$$S_{XY}(\omega) = \int \overline{X'(t)Y'(t+\tau)} \exp(i\omega\tau) d\tau; \quad \overline{X'(t)Y'(t+\tau)} = \frac{1}{2\pi} \int S_{XY}(\omega) \exp(-i\omega\tau) d\omega,$$

Where X and Y are two turbulent variables as function of time, with correlation as function of a lag time, τ , with a corresponding cross spectrum $S_{XY}(\omega)$ of frequencyω**,** Similar expression could be formulated for the spatial correlation of$\langle X'Y'(x_i + \delta_i) \rangle$ and its corresponding wave number cross spectrum, $SXY(k_i)$. Here the wave number analysis is different from the frequency analysis, in that the spatial lags, δ_l, and the wave numbers, k_i , are vectors. Taylors hypothesis is relating frequency to k_1 only, the wave number one along the mean velocity direction.

The spectra are in Figure 9 are scaled with the same scales as the profiles <u'w'>, <w'T'>, etc.- And are plotted versus a normalised frequency $n = fz/\langle u \rangle = k_1 z$,, with f in Hz, and, where we have again used Taylors hypothesis for the frequency-wave number relation, the z appears from the Monin-Obuchove similarity. (Kaimal et al, 1972).

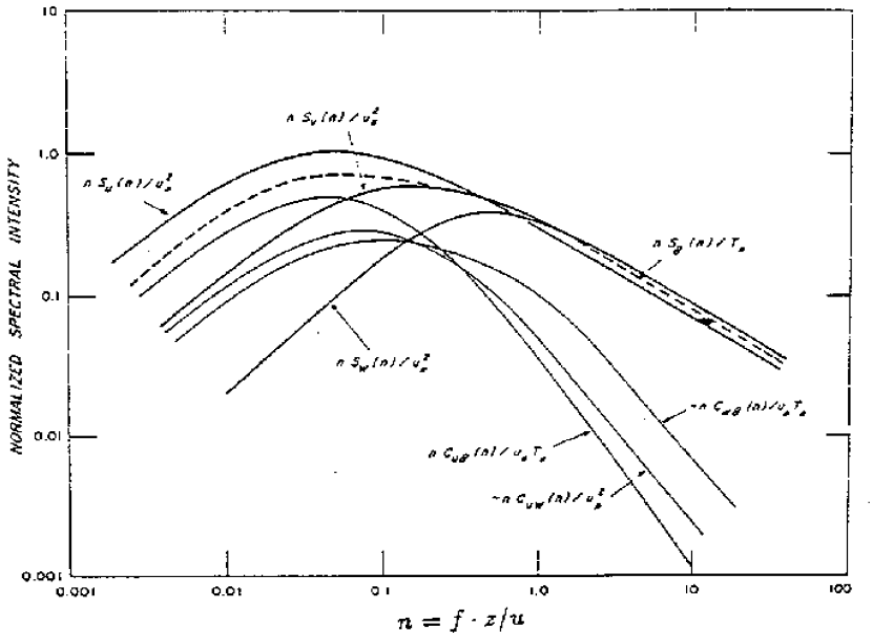

Figure 9. Neutral scaled ASL power and co-spectra from Kaimal et al (1972) plotted versus the normalised frequency n= fz/U. The spectra are scaled by the relevant Monn-Obuchov parameters defined in (7).

The spectra in Figure 9 are impirical and other spectral expressions exist, but there is a general concensus on their form and intensity, such that the different forms agree broadly on the behaviour of the spectra, although there are low ferequency differences as well that can be important in connection with some load modeling on structures (Andersen and Løvseth, 2010, Design Standards, 2017-11). The spectra vary systemantically with height through ther ABL and with stability in widely accepted ways. Olesen et al (1982), Højstrup, Man (1998)

At present, there is a strong activity of extending of profiles and turbulence expressions all the way through the ABL, and even further up. This is both because the growing wind turbines makes the information important and also because the breakthrough in the remote sensing technology, has made systematic data gathering in these heights possible. Some progress has been made, as indicated by the illustration in Figure 10. However, it is still a speciality in development, because the profiles aloft become sensitive to many new important scales, like the ABL height, but also on the detailed characteristics of the entrainment zone above the ABL.

An often used scale for strongly unstable condition, is a velocity scale constructed from the turbulent heat flux, to be used when the heat flux is more important that the momentum flux, and often in the upper part of the unstable ABL: $w_* = (h\langle w'\theta' \rangle g/T) \sim u_* (-h/\kappa L)^{)1/3}$, u_* will typically at most be a few tens of cm per secont,while w_* can reach several meter per second. Additionally , to the new scales entering the problem,the demands to homogenity becomes more severe, and several aspects of remote instationarity and inhomoneity, not really influencing the profile in the ASL, will influence wind speed and wind turning aloft, like e.g baroclinity and

remote changes in surface characteristica. We shall consider these aspect later. Here we present experimental and theoretical effort to describe the wind profile to greather heights .

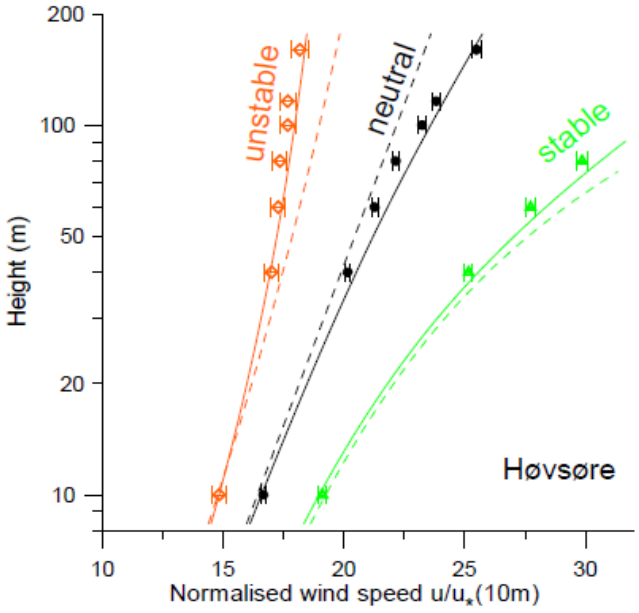

Figure 10. Newly developed models tested against data from the Høvsøre site in Denmark. The broken line are the extrapolations of the ASL models presented in Figure 7, the solid curves reflect models dveloped by Gryning et al. (2007), volving the boundary layer height and one more height scale.

We finally return to the concept of thermal stability, which as we have seen is a measure of the importance of the atmosphere's thermal statification relative to the wind shear dynamics the for the flow structure. In the SBL it can be described by the stability length L (7 and 8). Commonly used are the so called Richardson numbers, that measures the ratio between the potential and the kinetic energy across a layer. In the ABL it is mostly defined in terms of gradients of the mean temperature and the mean wind as shown in the following equation (14).

$$Ri = -\frac{g\Delta z}{\overline{\rho}}\frac{\Delta\overline{\rho}}{(\Delta U)^2} \sim \frac{g\Delta z}{\overline{\theta}}\frac{\Delta\overline{\theta}}{(\Delta U)^2} \sim \frac{gz}{\overline{\theta}}\frac{\Delta\overline{\theta}}{U^2} \sim \frac{g}{\overline{\theta}}\frac{\partial\overline{\theta}/\partial z}{(\partial U/\partial z)^2}, \qquad (14)$$

Where the first term is the basic definition stability in terms of density gradients for a layer of depth Δ, while the three last second forms are those most used in the ABL,and are based on a relation between the potential temperature and the potential energy. The third term characterising a layer from the ground to height z,is denoted the Bulk Richardson Number. while the 4th form is the differential form. Inserting the profile expressions in (12), Ri can be described in terms of the SBL formalism. But Ri is more general validity than for the the SBL. To be completely consistent with (7) we should have introduced water vapour into (12) as well.

4.1 Surface Characteristics of real ABLs

We shall consider characteristic real ABLs in the light of the ideal one considered in the former section. Characteristics of a flat homogenous land surface, a Marine ABL, the effect of moderate inhomegeneity, and finally steep surfaces and complex terrain.

To understand some of the differences, we must consider layers below the turbulent ASL, because this is vere the frictional processes resulting in a roughness takes place, and where the surface temperature is a result the heat flux properties. The roughnes lenth z_0 is the height , where the logarithmic profile extrapolates to zero due to surface friction. However, below a height of about $10 \cdot z_0$ the real profile is not logarithmic anymore, because of the molecular friction and because of the flow impacting on irregularities of the surface roughness elements.

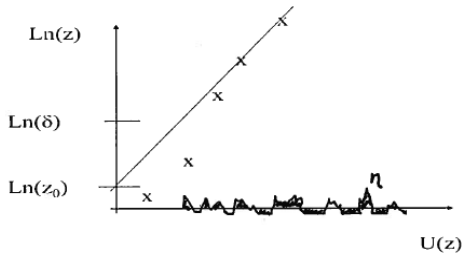

Figure 11. Extrapolation of the logarithmic profile down towards the surface below height of the viscous surface layer,δ. The logarithmic line is shown, while real velocities are indicated by x. Small scale irregularities, which we will denote roughness elements, are indicated.

Tracking the momentum transport through the viscous layer reveals that the momentum and heat transport to the surface is taken over by close to the surface can be written as:

$$\overline{-w'u'})_z = u_{*z}^2 = (\overline{\frac{p}{\bar{\rho}}\frac{\partial \eta}{\partial x}})_\eta + \nu(\overline{\frac{\partial u}{\partial z}})_\eta ;$$
$$\overline{-w'\theta'})_z = \nu_\theta(\frac{\partial \bar{\theta}}{\partial z})_\eta \qquad (15)$$

The real irregular surface as indicated on the figure and denoted, η (x,y), while ν and ν_θ are the molecular diffusivities of momentum and heat respectively. On the left hand side of (15) the transport taking place in the turbulent ASL have been indexed with a z. In the viscous layer ASL turbulence cannot exist due to the nearness of the surface, and the transport is taken over by molecular gradient diffusivity and for momentum also by the pressure perturbation around the irregularities. The correlation obviously becomes larger with steeper and sharper irregularities, roughness elements. If there is no roughness elements the transport is limited by the molecular diffusion, and a scale analysis indicates the $z_0 \sim \delta \sim \nu/u_*$. With roughness elements present the roughness becomes larger. On the other hand the heat transport in (15) includes no pressure term, since pressure appears in the momentum equation only. Therefore the transport of heat in the viscous sublayer is basically due to the molecular diffusion only, and z_{0T} ,and correspondingly z_{0q} , must be expected to be smaller than z_0, and more so, the more rougher the surface. As mentioned earlier typically $z_{0T}/z_0 \sim 0.1$ for rough surfaces.

Next we turn to the surface temperature θ_0, appearing in (8) and implicit in all our arguments about the effects of stability. The surface temperature is a boundary condition in (8) but it is as well a result of the energy balance

at the surface and controlled by processes above, on and below the surface. At the surface the energy balance per unit area can be written as (Budyko, 1974):

$$C\frac{d\theta_0}{dt} = NR + H + E + G\,, \qquad (16)$$

where, $C\cdot d\theta_0/dt$ the heat accumulation in a thin layer at the surface, with C being the heat capacity of this surface layer.

NR is the net radiation at the surface, consisting mainly of the incoming short wave radiation from the Sun and outgoing long wave radiation from the surface itself. NR is positive day time, most positive around noon, and it is negative during night, when the surface undergoes radiational cooling. Cloud cover, season and latitude is obviously important here.

H is the turbulent heat flux = $\rho C_p \langle w'\theta'\rangle$, cooling the surface when it is warmer than the air, and heating it when it is colder, typically due to radiation at night and day. Obviously it can reflect also changes in the air temperature due to advection, from (8) we have $H = = \rho C_p \langle w'\theta'\rangle \sim -\rho C_p (\theta(z)-\theta_0)\kappa u_*/\ln(z/z_{0T})$. E is the latent heat flux=$\rho L\langle wq'\rangle$, reflecting that the surface can regulate heat by evaporating water or condensing water vapor. Just as for temperature these processes can be driven by radiation, but also by advection.

G is the ground layer heat flux, which as all the other fluxes in (16) can be both negative and positive. But it will typically be directed downwards during day time, and upwards during night.

The value of q_0 at the surface is driven by surface mass balances similar to the surface energy balance for temperature. For humidity there are of course no radiation terms, on the other hand there are two interacting balances, one for liquid water and on for water vapor, with a strong dependency on the soil type and its water content, and- if vegetated- on the vegetation types, all with different root systems and different strategies for exchanges with the atmosphere. We shall not dwell further on these complexities in this context. We just notice that if the surface is wet, it all simplifies to that q_0 can be derived from the saturated water amour pressure at the surface, e_s, where $e_s(\theta_0)$, since at the surface $T_0 = \theta_0$.

4.2 Homogenous Land ABL

For a flat fairly homogenous land surface the ABL has a number of characteristics of relevance for the detailed use of the equations and models, described in section 3.

The energy balance at the ground (16) generally results into a significant diurnal and annual cycle of the surface temperature and the thermal stability of the atmosphere with instability during day, and stability during night, and the role of advection is less apparent. With this follows also a tendency to have deep ABLs at day time, following (10), and shallow stable night time ABLs. The diurnal variation of the surface temperature, penetrate down to about half a meter in to the soil, where the amplitude vanishes, hence only a shallow soil layer, with relatively little heat capacity, is involved in the diurnal heat exchange with the surface- somewhat deeper for the annual scale. For higher wind speeds the stability is often forced towards neutral by the roughness generated turbulence, even with fairly large heat fluxes. From (9) is seen that a given Geostrophic wind will result in a

larger u_* the larger is the z_0. From (7) is seen that we can write $z/L \sim z\kappa g T_*/ u_*^2$, which diminish with increasing u_*. The numerics is such that we will have $z/L \sim 0$ for moderately to high wind for characteristic land surface roughness.

The roughness elements of the surface consist mainly of either stone like fragment, ranging from pebbles over boulder and houses, or vegetations ranging from the tiniest leave to major forests. For a surface of simple roughness elements, one can often use Lettau's formula:

$$z_0 \approx 0.5 \cdot h \cdot S / A,\ A >> S \qquad (17)$$

Where h is the height of the roughness element, S its crosswind area, and 1/A is the surface density of roughness elements (Lettau, 1969). For densely placed vegetation, one can often use a simple z_0 proportional to the vegetation height, and additionally introduce a so called displacement length, d ,also proportional to the height of the vegetation, with different coefficients of proportionality for different types of vegetation, see Figure 12.

.

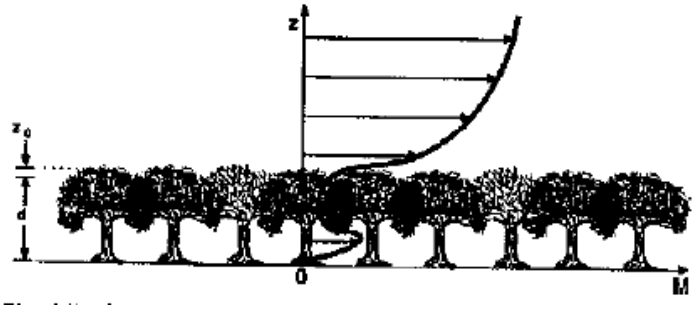

Figure 12 A forest canopy, showing displacement height, d, and roughness length z_0 as being proportional to the canopy height. Additionally the wind profile is indicated. Clearly, only the wind above the canopy can be expected to be represented by an ABL profile. The displacement height indicates the "ground-level" for the ABL profile, while the wind inside has to be described by other methods (Stull, 1991).

Vegetation based z_0, shows some, although fairly weak variation, with wind speed, reflecting that the wind is moving straws, branches and leaves etc. Also some stability variation of z_0 has been proposed, reflecting the structure of turbulence eddies penetrating into the canopy (Zilitinkevich et al, 2009). Further, a clear dependency on the seasonal variation of foliage is found, as in Figure 12. For this kind of land roughness, the z_{oT} and z_{0q}, must be expected to be about 10% of the z_0, as in section 4.1.

Figure 6 points to a seasonal variation associated with snow cover, where such happens. The figure suggests a z_0 value of about 2 mm for a natural snow surface, which could then be the prevailing roughness for such surfaces during wintertime.

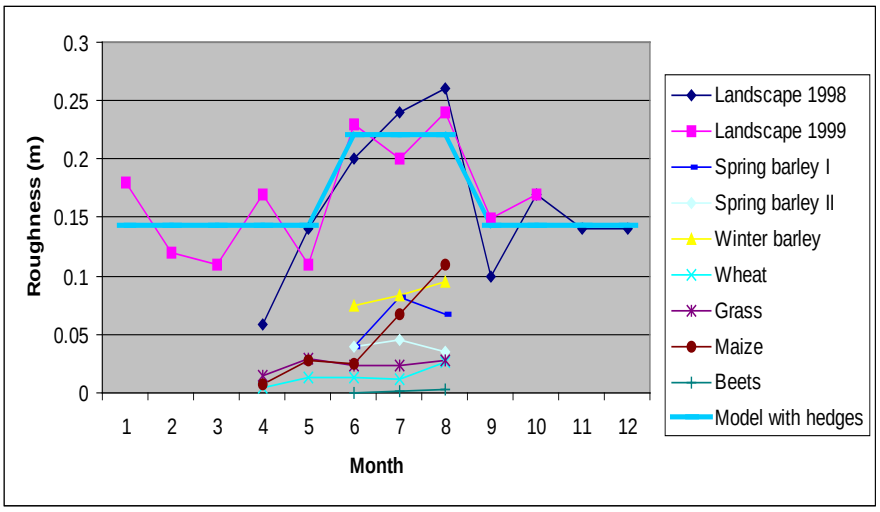

Figure 13. Measurement and modeling of seasonal variation of roughness for different types of vegetated surfaces (Hasager et al, 2003).

4.3 Homogeneous Marine ABL.

The marine ABL has distinct features compared to the land ABL. The water is semi transparent meaning that the radiational heating and cooling is distributed downwards. Additionally the water has extensive mixing properties. The surface waves and circulation systems, like the Langmuir Cells, combined with turbulence give rise to extensive mixing. Additionally, when heated the surface water evaporates, it will start sinking; now being heavier, because it retains the salt from the evaporated water. If the surface water cools, it also becomes heavier due to the cooling and sinks. All this give rise to an intense mixing in typically the upper 10 meter of the ocean. In the heat exchange with the atmosphere the water therefore constitute a very large heat reservoir that only can change its temperature slowly, and additionally has its own heating and cooling from the ocean currents. Indeed when an air mass moves over an ocean it always ends up at the temperature of the ocean. For these reasons the homogeneous marine ABL is always close to neutral. The diurnal radiation cycle shows very little influence on the water surface temperature, although it can be measured, but typical amplitudes are less than a few tenths of a degree (Pena et al, 2008). The annual radiation cycle on the other hand has significant influence on the sea temperature, because they involve enough heat to change both the temperature and the depth of the mixed layer. However, stable and unstable conditions happens over the ocean as well on shorter timescale, , but they are mostly transitional, associated with air masses moving across water surface with a different temperature, either coming from a nearby land or associated with moving weather systems. We shall return to these phenomena when coming to the inhomogenous and instationary ABLs.

The sea is also an obvious source of water vapor evaporation, indeed over the ocean since the q_0 is derived from the saturated pressure at the surface temperature. The ocean is also a source of liquid water in the form of sea

spray converting to marine aerosols. In wintertime the spray is the source of icing on ships and offshore structures.

The roughness elements over water mostly take the form of small steep waves of a wave length of around 5 cm, although momentum can be transferred also by larger scale breaking waves. The ocean surface is depicted in Figure 11. Since the roughness is associated with the waves and the waves are generated by the wind and modified by gravity, Charnock (1955) proposed that the roughness should depend on u_* and g. A slightly updated version of the roughness for water looks as follow:

$$z_0 = 0.11\frac{\nu}{u_*} + \beta(c/u_*, -)\frac{u_*^2}{g} \qquad (18)$$

where the first term reflects the molecular diffusion limit, discussed in section 4.1, when only few roughness elements are present. The coefficient, β ,denoted the Charnock constant, is currently considered a function of the phase c speed of the dominant waves and u_*, since the roughness elements will be mowing with the phase speed of the dominant waves in the direction of the wind. The term c/ u_* is denoted the wave age, because c increases with the duration of the acting wind$_*$. β is varying between 0.01 $_{\text{and}}$ 0.07, being smallest for mid-ocean mature waves with large phase speed. A "typical" value for regional seas is 0.015. β can be a function of other parameters as well: e.g. bottom topography, swells, both modifying the waves and their direction of propagation, and very high wind (e.g. hurricanes) results in foam covered waters that reduces β further (Makin, 1997).

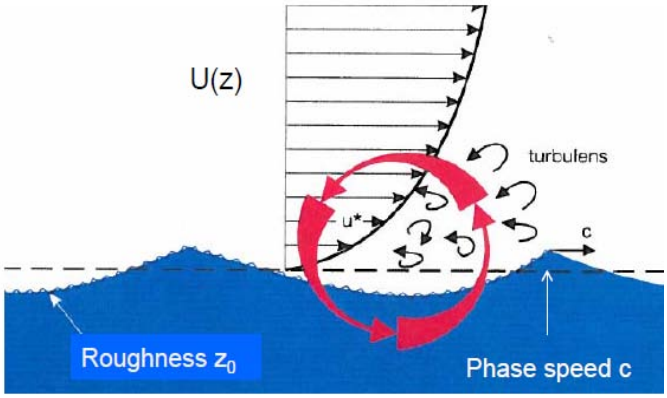

Figure 14. The wind profile close to the water surface, with the wave induced vorticity and the small scale roughness element riding on the larger scale waves, with a phase speed c.

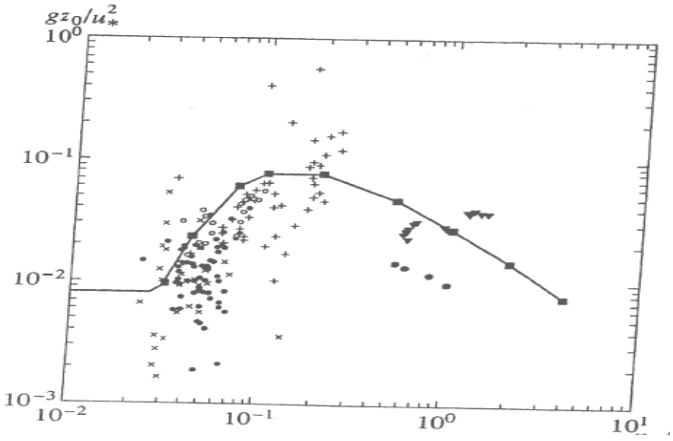

Figure 15. The Charnocks function, β is shown versus reciprocal wave age, $u*/c$. Typical wave ages in nature is between 5 and 30, Jones et al (2001)

In spite of the functions shown in (18) the roughness of the sea surface still remains one of the smallest, one can encounter in nature. This means that high wind speeds will be less efficient in forcing the stability towards neutral over water than over land, although also over water frequency of neutral stability increases with wind speed. Still high wind can be encountered associated with strongly stable flows over water, again reflecting an inhomogenous situation where warm air is advected over cold water, and the friction almost disappear. Again we shall return to this issue. Just as winter snow can modify the roughness of a land surface strongly, the winter will some part of the world cover the water with ice, see again Figure 6, and the roughness now will depend on the characteristics of the ice surface, ranging from extremely low for smooth solid ice, to quite rough for pack ice. The small z_0 also mean that the turbulence typically is lower over the water than over land, reflected also in a lower ABL height over water than over land. The small z_0 also means that the z_{oT} and z_{0q} are close to z_0 for low wind speeds, and start deviating only for rough pack ice or larger wind speeds, with rough sea.

4.4 Inhomogenous and instationary ABL

No ABL is strictly homogenous and simple models have been developed to handle the inhomogneity to organise the ideas about the complex subject.

Starting with an abrupt roughness change as despicted in Figure 16. Here the wind blows from a surface with one roughness over a surface with an other roughness. The stability is neutral. The turbulence associated with the new roughness growths into the upstream boundary layer by diffusion. This new

boundary layer is called and Internal Boundary Layer, IBL, because it growths within the already existing boundary layer.

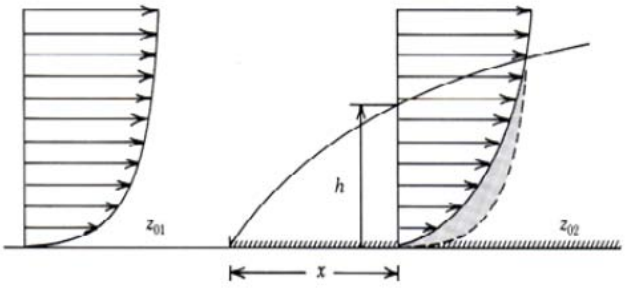

Figure 16. Description of the structure of the internal boundary, of height h(x), due to a step change in terrain roughness . Rule of thumb h~ 0.1 x.

$$\frac{dh}{dt} = \overline{u}(h)\frac{\partial h}{\partial x} = Au_{*0} \rightarrow \frac{\partial h}{\partial x} = \frac{\kappa A}{\ln(h/z_0)} \rightarrow Cx \simeq h\ln(h/z_0) \tag{19}$$

Where we have used that u (h) follows the logarithmic profile. C is found to be about 1. Notice, we measure u_* as u_* at the surface, because u_{*2} must be expect to vary with height in the IBL. The system works for both a smooth- to -rough transition, and the opposite, as long as one uses the largest roughness of the two in the IBL growth equation (17). With h(x) determined in (17), we can find the new surface the new u_{*2}, matching the upstream and downstream profile at h to yield. .

$$\begin{aligned} &\overline{u_1}(h) = \frac{u_{*1}}{k}\ln(\frac{h}{z_{o1}}) = \frac{u_{*2}}{k}\ln(\frac{h}{z_{o2}}) \Rightarrow \\ &\frac{u_{*2}}{u_{*1}} = \frac{\ln(\frac{h}{z_{01}})}{\ln(\frac{h}{z_{02}})} = \frac{\ln(\frac{h}{z_{01}}\frac{z_{02}}{z_{02}})}{\ln(\frac{h}{z_{02}})} = 1 + \frac{\ln\frac{z_{02}}{z_{01}}}{\ln(\frac{h}{z_{02}})} \equiv 1 + \frac{M}{\ln(\frac{h}{z_{02}})}; \end{aligned} \tag{20}$$

Equation (20) provides a very successful estimate of the ratio between the upstream and downstream u_* values with fetc, x, since h= h(x). Additionally it provides us with a way of characterising magnitude of roughness changes, through the factor M is the last term. From Figure 6 we get that the roughness change between a water surface and a smooth land surface with a $z_0 \sim 1$ cm has the same roughness change magnitude as the roughness change between the same land surface and a city or a major forest. Both roughness changes are associated with roughness ratio of about 100. We may also use the results to estimate, how wide a homogenous area that is needed for the assumption about homogeneity to be good. This is height dependend. The growth rate of the IBL given by (19) is slightly slower than h = 0.1x, meaning the measuring height should be less than 10 times the fetch, x, to feel the new IBL. It can shown that the height below which the flow is in approximate equilibrium with the new surface is about 0.01x, meaning that we will need a homogeneous new fetch of 100 times the measuring height to consider the upstream conditions homogeneous. Under all circumstances the demands to a homogenous fetch, depends on the measuring height. This is one explanation of why it has been found to be more difficult to obtain consistent estimates of the profiles aloft. For example the profiles obtained up to 200 m in Figure 7, demands homogeneous fetches of 20 km to be in equilibrium with the underlaying surface. Uncritically, we could extend the theory to a full ABL, find as a rough estimate we should have a fetch of 100h to have a new equilibrium situation.

From (20) one can estimate also the ratio between the upstream and down strean wind speeds. Unfortunately, the formulation is wrong for very large fetches, where it predicts the u_*-ration becomes unity, which is not in according with the resistance law for a new ABL with the new z_0. Also stability effects are not included. Both deficiencies can be repaired, but the results miss the appealing simplicity of (20), and will not be treated here.

Instead we turn towards the flow over low hills: As the flow approach the hill a pressure perturbation develops, reaching both upstream and down stream and breaking the air on the front slope and back slope of the hill and and developing an acceleration on the top of the hill.

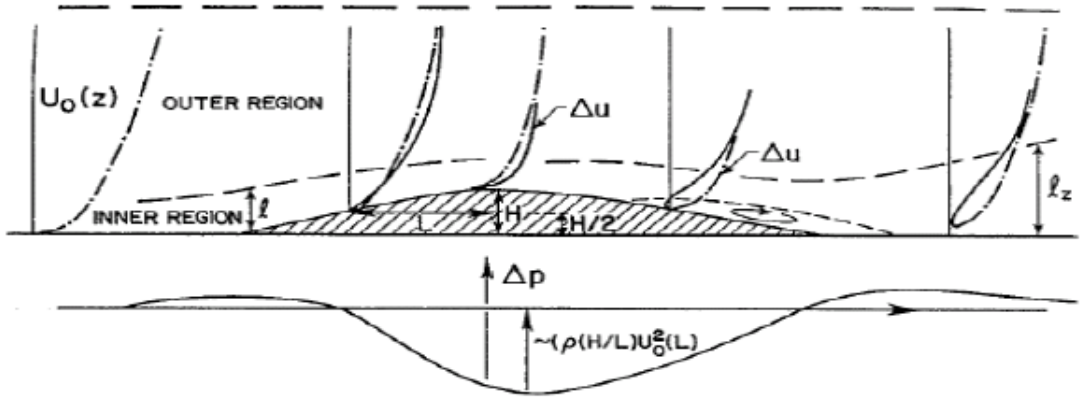

Figure 17.the principles for flow over low hill according to Jackson and Hunt (1975) from Hunt and Simpson (1992), with the width, L, the height, H, defined.

The flow over the hill is described for three regions in the vertical. At a height L the pressure perturbation has dissapeared, and the flow is undistorted. In the inner region the maximum flow perturbation takes place, while the wind is still forced to zero at the ground. Therefore, this is the region with the largest wind shear. The maximum wind pertubation takes place at the top of the inner layer, and gradually decreases to zero at the height,L. The hight of the inner layer is of the order of 0.1 L, and the pertubation of the top of the hill, the socalled relative speed up, is found as:

$$\frac{\Delta u}{u_0} \approx 2\frac{H}{L} \qquad (21)$$

(Troen and Petersen(1989) has developed the theory into a Fourrier form, allowing one to build an arbitrary landscape as a supperposition of low hills, which when combined with the roughness changes, becomes the model in the WAsP system(Troen and Petersen(1989) . If the slope becomes too large, of the order of 20%, flow separation can develope on both the upstream and the downstream slope, and the simple relations break down

We next turn towards the situations which are driven by a changing heat flux. Her we start with the diurnal cycle for a horontally homogeneous area at midlattitude, where the boundary layer show obvious diurnal changes. As we have discussed the changes will be smaller if the wind is high, and the atmosphere is cloudy, than when the wind is low and the sky is clear, but it will always be present, and limitting the degree of stationarity one can expect for such a surface. A similar changing rate can be found in frontal passages, which takes a time of the order of one day or longer.

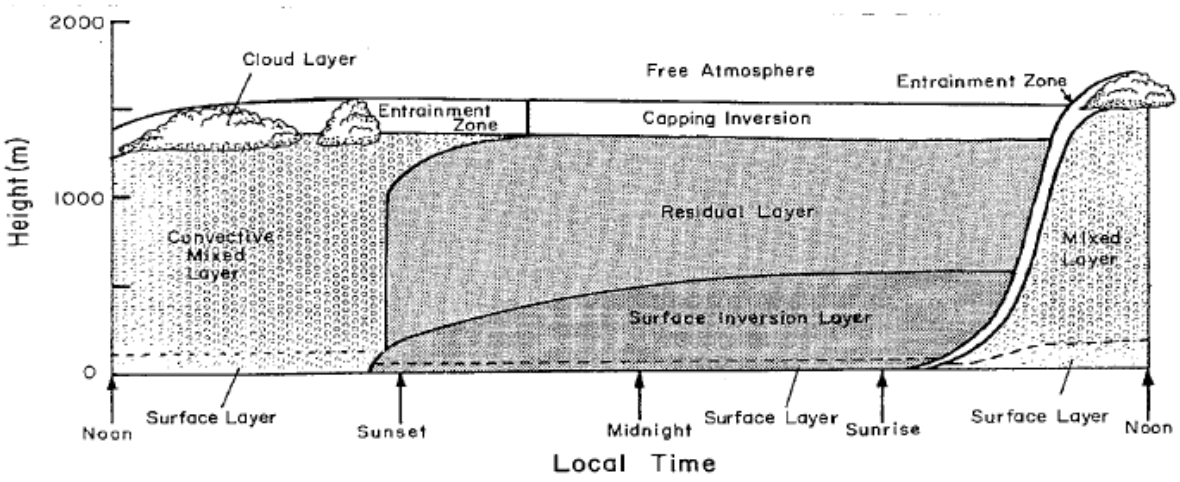

Fig 18. A heat flux driven diurnal change of the ABL fo a homogeneous midlattitude land surface (Stull, 1991)

We next turn towards an IBL controlled by the surface heat flux, where the IBL, here denoted TIBL, growths against a stable upstream ABL. Here, we can use the growth of the unstable boundary layer equation in (10), also depicted in Figure 18, for the growth of the day-time ABL, just assuming that the upward heatflux now happens as function of fetch, x, instead of time, inserting t= u/x in (10). A more comprehensive description of these types of models are found in Gryning and Batchvarova (1990). The situation can happen for both land and water surfaces, being dependent on differences in surface heat flux and/or surface temperature of the two surfaces involved. However, it is quite easy to imagine it developing at a coast line, because the surface temperature of the land and the sea quite often is different, due to the two surfaces different response in the surface energy budget (16) on a diurnal scale. As the time and space scales for such coastal system increase, the differential heating between two surfaces, will influence the atmospheric dynamics, because air will tend to rise over the relatively warm surface and sink over the colder area. The resulting circulation is called a land- sea breeze system. At night the land cools relatively to the sea, and the flow reverses. The land-sea breese is best known is of the breeze systems. However, breese systems occur also as breeze systems around major cities, because of the "urban heat island" effect. When the spatial scale of a land-breeze system increase to continental scale, one talk about Monsoons, which will typical be seasonal rather than diurnal. However breeze systems of many scales can exist at the same location, and will often interact.

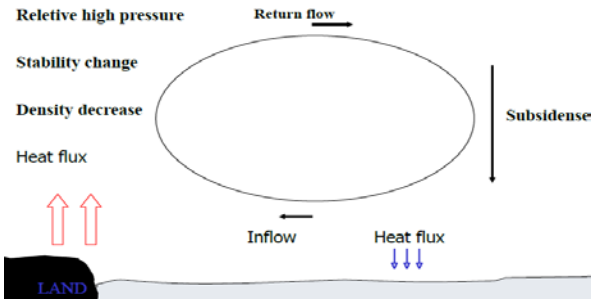

Figure 19. Land –sea breeze system, where a hot land results in rising air, while sinking air over the relative cold water results in a sinking air.

A more complex situation appears for a transition from an unstable ABL passing over a colder surface, where the more intensive unstable ABL has to decay before the stable IBL can establish itself. Also, these situations occur quite often in some coastal areas.

Especially the transition from relatively warm unstable/neutral land ABL into a stable IBL over the water (Melas , 1998). Lange et al.(2004)has been studied. Several things happens. The air gradually looses heat to the water and reach the water surface temperature at the inteface, where a small neutral layer establishes itself. This neutral layer slowly groths up throughthe stable IBL, until all the original temperature gradien between the two air masses is concentrated at the top of a new boundary layer that however can take many hundred kilometers to estabilsh itself.

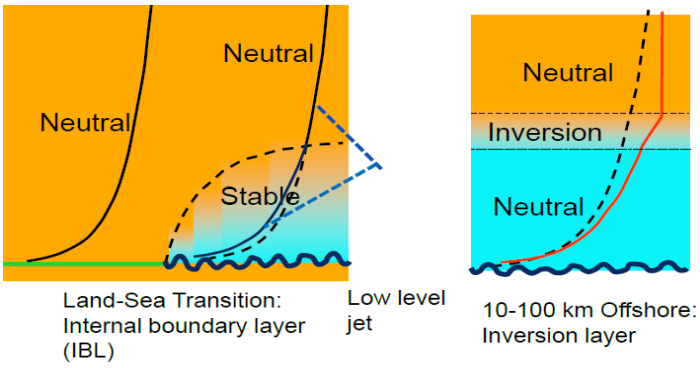

Figure 20. Warm neutral air flowing over cold water, and develop a stable IBL, SIBL, gradually transitioning to a neutral ABL with an inversion on the top. over the water for off-winds. Lange et al (2004). The broken triangular line indicates the possibility for a Low Level Jet at the transition.

A Low Level Jet may happen in the transition between land and water, because the surface friction in the boundary layer suddenly disapears, for the air crossing the coastal line. Considering (1), we see that the wind above the boundary layer is unchanged,friction is unimportant here. The velocity within the ABL must accelerate because the the friction is reduced, finally the wind still has to go to zero at the surface. It is a transitional phenomenon that gradually disapears as the full profile and stress profile reasserts themselves downstream from the coast line. These Low Level Jets can appears, wherever the surface stress reduces because of increasing stability or decreasing roughness or both. It is quite well known over the nighttime Plains of US, wher they are result of the growing night time stability.

The heat/temperature controlled IBLs may happen also especially over water, when synoptic air masses are advected over relatively cold or warm water. Here especially, the second one, will give rise to a thermally induced convective IBL, which over the water typically will be associated with meso-scale structures like rolls and cells.

The large scale temprature differences may allso influence the basic equation system in (1). In this system only pressure was allowed to change to ensure a pressure gradient and thereby a Geostrophic Wind. If the large scale temperature is allowed to change horizontally, meaning that T_s and T_a changes together in Figure 4, the simple relation for the Geostrophic wind in (3) changes to:

$$G = (U_{1G}, U_{2G}) = (-\frac{1}{f\,\overline{\rho}}\frac{\partial \overline{p}}{\partial y} - \frac{gz}{f\,\overline{\rho}}\frac{\overline{\partial} T_l}{\partial y}, \frac{1}{f\,\overline{\rho}}\frac{\partial \overline{p}}{\partial x} - \frac{gz}{f\,\overline{\rho}}\frac{\partial T_l}{\partial x}) \qquad (22)$$

In (22) the original G is present at the surface only, and the deviations are seen to increase with z. Also they will influence both the magnitude and the direction of the Geostrophic wind for baroclinic situations. Indeed a low

level jet can result from this type of baroclinicity as well (Garreau and Munoz, 2005). The subscript l refers to that the temperature must be considered a layer average. The thermal contribution is often called “The Thermal Wind”.

We finally mention coast line changes that firstly happens in the water, but may still influence the air above the water: For deep water coasts, currents and wind may cary the surface water outwards, and upwelling of deeper colder water replaces it closer to the shore. This means that the flow approaching the land is in the process of cooling and developing a stable internal boundary layer over the coastal water, as in Figure 20, before making landfall. A well known example is the Californian west coast upwelling sea- breeze system. For shallow coasts on the other hand the coastal water reflects the land surface temperature more, because the radiation balance reach all the way to the bottom. Additional enhances wave breaking may also enhance the mixing through the water of both momentum and heat (Johnson et al,1999).

4.5 Complex terrain

With complex terrain, we will understand a terrain composed of random randomly steep slopes. As we discussed in the former section, we can in the principle models flow over terrain composed of random slopes and roughness changes at least as long as the thermal conditions are less important in the WAsP modeling system (Troen and Petersen, 1989). But if there are too many steep slopes in an area, there are no simple models available for the flow computation. For such work a system RIX, Ruggedness IndeX (Mortensen and Petersen, 1997) has been developed that compare steepness around a meteorological station, from which the data are extrapolated to potential wind turbines sites, with the steepness of the potential sites. Hereby it has been possible to estimate and reduce the errors of the simple flow models, associated with larger steepness somewhat.

Often the varying terrain will give rise to different temperature fields, and if slopes are additionally of a height that is comparable or larger than a typical boundary layer height, the boundary layer can break down into several different boundary layers, at different levels above grounds or in different parts of the terrain. Therefore the diurnal radiation changes will modify different terrain parts differently. Figure 18 show and example of the diurnal change for a simple valley.

At night drainage flow of cold air down the mountain dominates, while a valley wind upslope of the sun heated slopes dominate in the late afternoon. The morning shows upslope flow on the part of the slopes that is reached by the sun, while down slope drainage wind prevails in the valley, not yet reached by the sun. The depth and strength of the flows can vary from deep and strong catabatic flows down stream to high winds upslope, down to shallow weak breezes in both directions. Obviously such flows can also exhibit sharp gradients in all direction as well a remarkable unsteadiness. The detailed flow structure will depend both on the solar input and also on synoptic pressure gradients across the landscape. Again, they depend on the detailed orientation of the slopes of the landscape. Therefore measurements must be recommended combined with modeling if detailed knowledge about such flows is required.

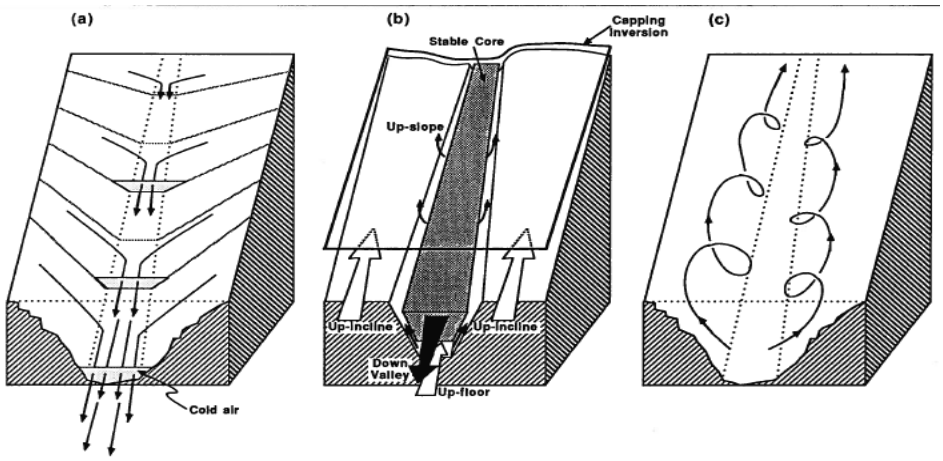

Figure 21. Three –dimensional picture of idealized local mountain circulations (a) at night, with cold air drainage, (b) morning with mixed up-and down slope flows, dependent on sun-rise , and (c) afternoon up-slop flow along the sun-heated slopes. (Stull, 1991).

4.6 Boundary Layer Climatology for Wind energy

Until now we have discussed the processes controlling the different boundary layer parameters and how the processes and parameters were forced by processes and conditions outside the ABL. The resulting climate at any location develops from a specific local mix of the processes and forcing described above, and must be determined either from measurements or integrated modeling.

It is important to limit the scope of such a climate study, one starts by specifying the focus, which is here offshore wind energy, meaning that one needs sufficient site specific environmental data for wind resource estimation and for establish the external conditions for the design or choice of turbine type. The data base can be established using existing data, new in situ measurements or modeling- or combinations of all these. There will be considerations about" Need to know and nice to know" and about the price and project duration for the different solutions.

For wind resource estimation wind speed and direction distribution at hub height is called for based on at least one year of data, since a year is the longest simple cycle in the climate, and preferably several years to account for the known inter-annual variability. Nice to know would be some stability information for comparison with models, since the offshore site is likely to be in a coastal zone for some wind directions, where conditions are influenced by the nearby land. However, pressure and temperature and humidity provide also the air density influencing directly the wind resource.

Next we come to the effort to establish environmental data for design basis and turbine details. The required statistics are summarized in Bredmose et al (2012) and detailed in the Design Standards (2007-11). For load estimation one needs to establish hub-height distributions of turbulence intensity and shear at the location and estimate extreme values of these parameters see Figure 8.

For an offshore site, also the wave climate has to be established, both with respect to wave height and wave direction This is not to estimate the roughness, but to estimate the wave loads and combined wind- wave loads on the wind turbine and foundation, and identify situations where the wind directions are different from the wind direction. The wind and wave extreme load analysis are formulated in terms returns periods of 1 to 100 years, utilizing Gumbel statistics (Bredmose et al, 2012), and in term of joined distribution for wind and waves.

Some of this information can best be obtained on site, and here the new advances of the LIDAR technology (Pena et al, 2012) have made it possible, and economically feasible, to have in-situ measurements off shore at larger heights than before, corresponding to the hub-heights today. But aside from the prize of offshore measuring stations, also the necessary project duration for obtaining the long return period estimates necessitates use of other data of other types, either long term measurements from nearby sites, that can be model translated to values at the site, or full scale model generated data. This has for some time been used for wave data, and can now be used on wind and other meteorological data as well, with the progress of meso-scale meteorological models to compute a sufficiently detailed climatology based on a climate from Reanalysis Data as (Haman,2012). Some available Global Reanalysis data bases are listed in Figure 22,

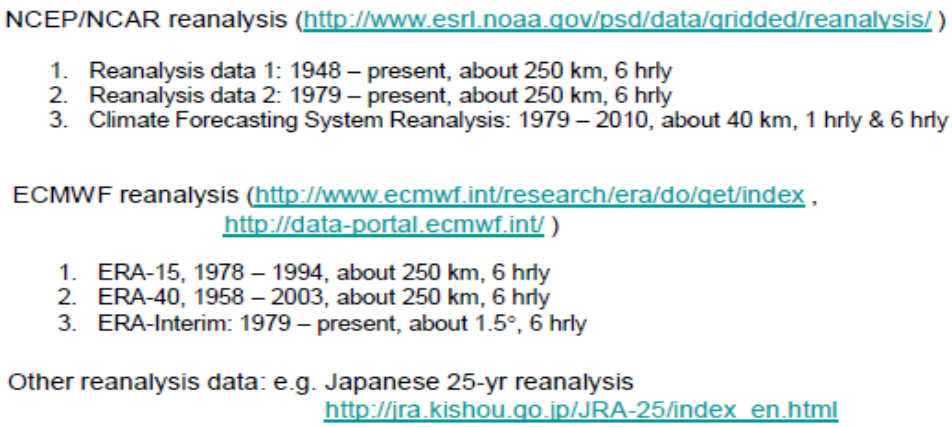

Figure 22. Different Reanalysis sets, with start time, and horizontal grid size and time resolution. The vertical resolution corresponds to 20-30 levels.

Stability (Temperature and humidity) and other possible data are here again “Nice to know”, for the same reasons as for the wind resource estimation.

Finally we mention that is quite normal that wind farm operators keep a meteorology mast running when the farm has started to operate, both to support the monitoring of the farm performance, and to support the service and maintenance function.

5. The Boundary Layer Climate for the Southern North Sea and Southern Baltic Sea off-shore regions.

Figure 23 shows the South eastern part of the North Sea region with the Southern part of the Baltic Sea with an annual mean wind in 100 meters height. We shall discuss the climate for this region in the light of the ABL discussions in the former section. The area is situated in the West Wind region, meaning that westerly flow occurs often, but all wind directions are important. The figure illustrates this with that the most windy regions are at the North West corner, where the flow comes around Scotland from the North Atlantic and across the North Sea. Therefore generally the wind over the North Sea is higher than in the Inner Danish Waters and the Baltic. However, the central area of the Baltic shows almost same mean wind as much of the North Sea, showing that the wind approximately return to equilibrium with a new water area, the Baltic water, after a fetch of 30-60km from land , in according with the discussion about roughness changes in section 4.4. Data in 100 meter should be in equilibrium with the new surface after 10 km according the ASL theory described in the section, but if we wish the full boundary layer to be in equilibrium we have refer to the boundary layer height, been 300-600 m.

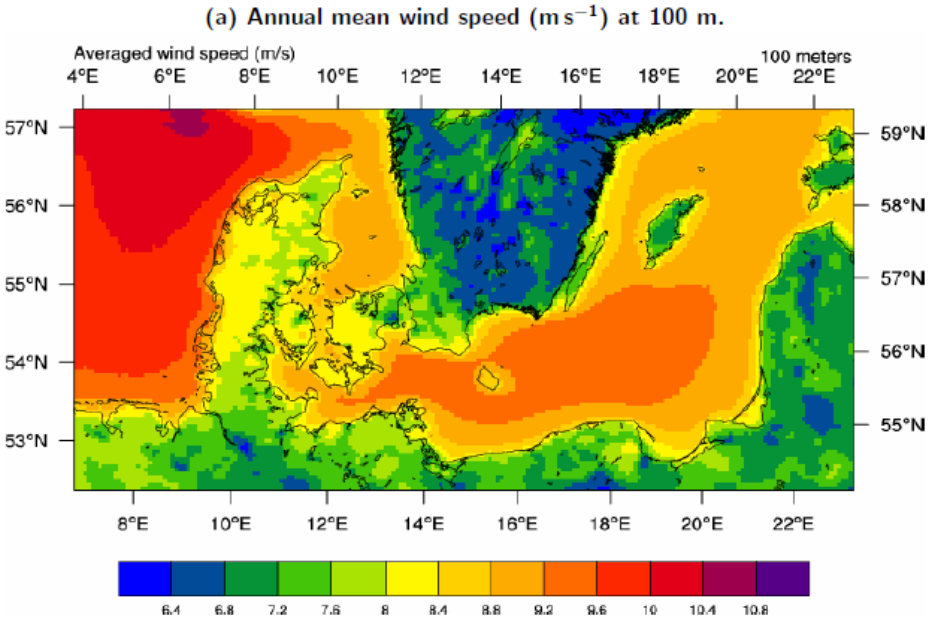

Figure 23. Annual mean speed at 100 meter estimated using meso-scale modeling. WRF and using Reanalysis Data 2006-2011 from Hahmann et all (2012). The higher mean winds over the North Sea are seen.

Proceeding to the general climate within the range of the figure , the North Sea coast has a typical maritime coastal climate, with relatively little difference between summer and winter temperature and a higher frequency of overcast and precipitation, and fairly windy, snow and ice exist but infrequently, and never on the North Sea itself. As one moves East the climate becomes gradually more continental, with larger seasonal temperature differences, less windy, typically spring and fall becomes shorter. Summer and winter are more intense. The snow cover of the land becomes more frequent.

The land region is fairly flat and with smooth hills and mountains, although the mountains of the Scandinavian Peninsula is situated just north of the region, and influences the weather patterns also into the region. This means that flow simulations over land of the region do not need to handle complex terrain provided the model grid is not extended over the Scandinavian mountains. The cloud cover is about the same on an annual basis, but in the east there is a stronger seasonality also in cloud cover with minima in the high summer and winter. Therefore, the radiation terms in the surface energy balance are more important over the easterly part of the region than the westerly, implying a stronger diurnal cycle as well, see section 4.1, in spite of that both the Eastern and the Western part of the region is at the same latitude.

The surface temperature of the two seas of the region have some significant differences., as illustrated in Figure 23, The North Sea is connected to the Atlantic Ocean and has its own heat supply through the Gulf Stream that heats the nearby lands and reduces the amplitude of the seasonal temperature change. The Baltic Sea on the other hand has its main water supply from relatively cold river water being colder in average than the North Sea., but being more landlocked the seasonal differences are larger, just as for the inner Danish Waters. Detailed inspection of the figures reveals that although the seasonal difference is larger, only in summer is the temperature higher than for the North Sea. The figures also reveal that the surface water seems to be warmer in the Southern part than along the Northern coast. One of the reasons for this is that the Baltic Sea has two counter clock rotation gyres that caries colder water from the North down along the Northern coast and out through the straits, while part is mixed with incoming water and flows along the Southern coast. Additionally the Southern coast has inflow from the warmest rivers in the Baltic region (Håkanson, 1991).

Irrespective of its variation the temperature of the Baltic Sea surface, the water of the Baltic Sea tends to be colder than the land from. Stedman et al (1997) concludes, based on 5 years measurements on a Gotland peninsula that on an annual basis the Baltic Sea ABL is stable about 2/3 of the time at 100 meters elevation, although the sea temperature is higher than the land temperature part of the winter. The largest temperature difference between land and sea is reached in the spring early summer at all coast in the region, but most extreme in the Baltic Sea. Over the Baltic Sea, we must therefore expect situations with the type of stable internal boundary layers as depicted in Figure 20, quite often. That means layers that appear neutral to slightly stable at lower heights, and gradually gets more and more stable with increasing height. Indeed the figure was prepared to explain the behavior of offshore data from a site south of the Danish Baltic Sea Island, Lolland (Lange et al, 2004). It will be interesting to get a validation of the phenomenon from independent data and analyses from the measuring masts that have been established in the region.

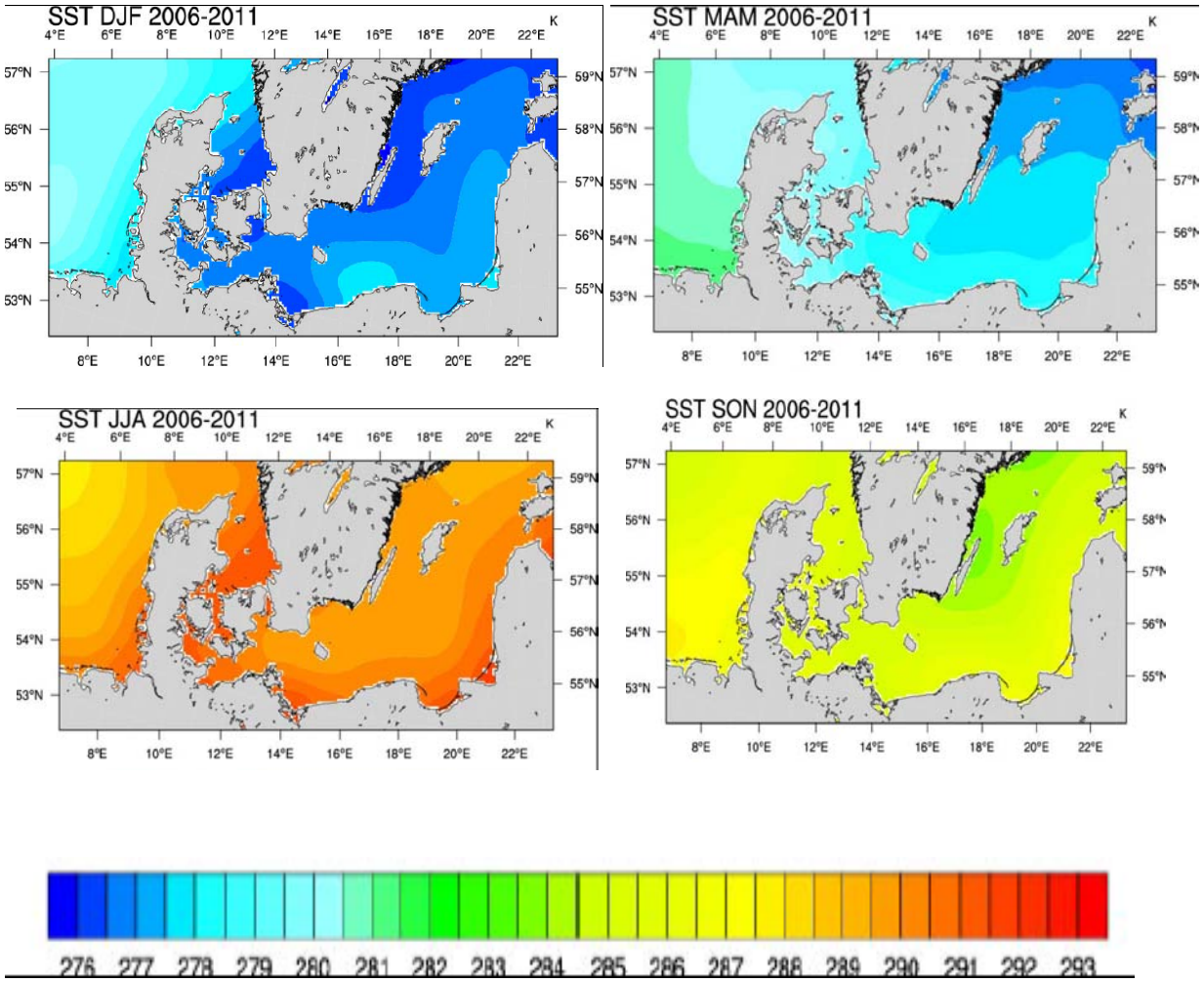

Figure 24. Surface temperature of the Baltic area the four seasons, indicated by months- The relatively constant temperature of the deep North Sea for different season is seen. As is the cool path seen as is the cooling of the Baltic (Private communication A. Hahmann and Hahmann, 2012)

In spite of the relative cold winter weather for the Baltic region and the brackish water there is little indication of a higher water ice frequency in the Southern region than for the Inner Danish waters, where the normally indicated frequency of ice is once every four years (Håkanson, 1991). However the icing frequency is likely to be considerably higher over the Baltic than over the Inner Danish waters, and virtually non-existing over the Southern North Sea.

6 Summary

We have allmost entierly avoided discussions of the different measureing systems in this presentation and concentrated on meteorological climatological aspects

We have summarised knowledge about atmospheric boundary layers, starting with the simplest ideal form, being statistically stationary and horizontally homogenous. We have thereafter introduced aspect of reallity

into the picture, considering stability and unstability, typical terrestrial boundary layers and marine boundary layers, and the important points of instationarity and inhomogeneity.

Over land we have seen that stability changes have a clear diurnal cycle, the importance of which becomes the smaller for the boundary layer structure, the higher the wind speed and the larger the cloud cover. On the other hand the thermal properties become more and more important the greater the height within the boundary layer. Over water stability is more associated with advection of air masses than dayly variation of insolation. On the other hand high wind does not force the stabilty towards neutral to the same degree as for the terrestrial boundary layers.

When the surface change the boundary layer reacts by forming an Internal Boundary Layer. Orography changes induced a presure perturbation that reach out in all directions within a range of the same scale as the width the terrain change. The pressure pertubation also perturbes the oncoming flow. Changes due to roughness and thermal changes on the other hand diffuse into the flow as it moves across the surface. The transistion zone for these changes will typically be of between 10 and 50 kilomer before a new boundary layer estabishes itself as a homogeneous boundary layer. The the highest levels in the boundary layer reach equilibrium the latest. The stable internal boundary layer over water for offshore flow takes the longest fetch to reach equilibrium up to more than 100 km, meaning for example that an enclosed sea as the Baltic Sea, with relatively cold water, must be consisdered intierly coastal.

We find that for complex terrain some general methodologies are possible, but one must expect to have ito nvest more specific studies for projects within such areas, before having sufficient information.

Finally, we compare the two regional seas of the region, the Baltic and the North Sea, in the light of the discussion of the ABL in the rest of the manuscript. The main differences are derived from the large scale features of the two sea, The North Sea region with an additional Gulf Stream heat input, is relatively mild coastal maritime climate. This becomes more continental as we move east along the Baltic shore, where the Baltic Sea additonally is fed by colder making it fairly cold. We conclude that there is a high probability of transient stable internal boundary layers over the Baltic Sea. It would be interessant to see it confirmed by independend data and analyses, from the measuring station in the region. Wind- wise the Southern Baltic Sea seems very similar to the Inner Danish Waters, but with a larger open high wind area in the center, where winds get closer to the North Sea level.

Notation

Reference to equations or figures.

A: Coefficient in the resistance laws (6) and an entrainments coefficient in (10), area (15), coefficient of proportionality in (17)

ABL and ASL; Atmospheric Boundary Layer and Atmospheric Surfaced Layer (Section 1)

α : Power in power law wind profile (9), Geostrophic angle (6)

B : Another coefficient in the resistance laws (6)

β: Charnock's coefficient as function of wave age in (16)

C: Surface heat capacity in (14), coefficient of proportionality in (17)

C_p: The heat capacity at constant pressure for air, defined first time on p.3

c : Phase velocity of surface water waves (16)

δ: Length scale lag-length on p14, height of interfacial layer Figure 10.

E: Latent heat flux (14)

e_s: $e_s = e_s$ (T) saturated water vapour pressure in the atmosphere.

η: Detailed surface height (13)

F: Unspecified function used in (11) and in deriving (10)

F: Coriolis parameter (1)

G = U_{1G}, U_{2G}: : Geostrophic wind (3), Soil energy flux (14),

g: acceleration due to gravity (1)

H: Height of hill (Figure 14), turbulent heat flux (14)

h: height of ABL, and height of IBL (Figures 4 and 13), height of roughness element (15)

IBL: Internal Boundary Layer (Section4.4)

κ : v Karman constant in Monin-Obuchov turbulence description (6)

ψ(z/L): Stability functions for profiles (8).

L : Monin-Obuchov stability length scale (7), width of the hill (Figure 14), heat of evaporation, p.4.

Γ: The dry adiabatic lapse rate (2).

NR: Net radiation (14)

ν, ν_θ: Molecular viscocity and heat conductivity (13)

ρ : density of air (1)η

p : air pressure(1)

q, q_0 : water vapour mixing ratio defined as density of water vapour/ air density, surface value of q (1)

q_*: Turbulence scale for q (7)

S: Cross wind area of roughness element (15)

σ: Standard deviation 811)

T: Temperature in K. (1)

$T*$ Turbulence scale for T or θ (7)

t: time (1)

Θ, Θ_0: Potential temperature in K, surface value of Θ , (2)

$U_i = u_1, u_2, u_3 = u, v, w$: Three components of the wind velocity.

$X_i = x_1, x_2, x_3, = x, y, z$. Three spatial coordinates.

z_0, z_{0T}, z_{0q} : Roughness length for u, T and q..

References

Andersen, O.J. and J. Løvseth (2010): Stability modifications of the Frøya wind spectrum. Journ. Wind Engeneering Industrial Aerodynamics, 236-242, 2010.

Bodyko, M.I., 1974. Climate and Life. International Geophysical Series, Vol. 18, Academic Press, New York, 508p

Bredmose, H., S.E.Larsen, D. Matha, A. Rettenmeier, E. Marino, L. Saettran (2012). D2.04: Collation of offshore Wind Wave Dynamics. MARINET Report, EU-FP7 Grant no. 262552, 50p.

Brutsaert, W.H., 1982: Exchange processes at the earth atmosphere interface. In: Engineering Meteorology, Ed. E. Platte, Elsevier, 319-369.

Design Standards, 2007-11.

IEC 61400-3: Wind turbines- Part 3: Design of offshore wind turbines, 2009

DNV-OJ-J101. OFF SHORE STANDARD: Design of offshore wind turbine structures. DNV, 2007.

ABS(American Bureau of Shipping), Offshore Wind Turbine Installation, American Bureau of Shipping, 2010

ABS(American Bureau of Shipping), Design Standards for offshore wind farms, American Bureau of Shipping, 2011
IEC 61400-1, Design requirements, 2008.
IEC 61400-1, Design requirements-amendment1, 2010

Garreaud, R. D. & R. Munoz, 2005. The low level jet off the subtropicalwest coast of South America, Structure and Variability. Monthly Weather Review, 133, 2246- 2261,

Gryning, S.E. and E. Batchvarova,1990: Analytical model for the growth of the coastal internal boundary layer during onshore flow. Quart. J. Roy. Met. Soc., 116, 187-203.

Gryning, S.-E.; Batchvarova, E.; Brümmer, B.; Jørgensen, H.E.; Larsen, S.E., 2007, On the extension of the wind profile over homogeneous terrain beyond the surface boundary layer. Boundary-Layer Meteorol. 124: 251-268.

Hahmann, A. N. , J. Lange, A. Peña and C.. Hasager: The NORSEWInD numerical wind atlas for the South Baltic, DTU Wind Energy-E-Report-0011(EN).

Hasager, C.B.; Nielsen, N.,W.; Jensen, N.O.; Bøgh, E.; Christensen, J.H.; Dellwik, E.; Søgaard, G.. (2003), Effective roughness calculated from satellite-derived land cover maps and hedge-information used in a weather forecasting model. *Boundary-Layer Meteorol.* v. 109 p. 227-254

Hunt, J.C.R. and J.E.Simpson, 1982:Atmospheric Boundary Layers over Non-Homogeneous terrain. In: Engineering meteorology (E.: E. Plate) Elsevier, Amsterdam. 269-318.

Håkanson, L. (1991) The Baltic Sea Environment. Session 1: Physical Oceanography of the Baltics. (ISBN 91-506-0876-2) The Baltic University Programme, Uppsala University, Swedem, 35 p.

Højstrup, J., 1982: Velocity spectra in the unstable planetary boundary layer. *J. Atmos. Sci.*, **39**, 2239-2248.

Jackson, P.S. and J.R.C. Hunt, 1975: Turbulent wind flow over a low hill. J. Roy. Met. Soc., 101, 929--955.

Jones, I S F, Y Volkov, Y Toba, S Larsen, N Huang, M Donelan (2001). Overview. Chapter 1 in: Wind stress over the ocean (Ed. I.S.F.Jones and Y.Toba). Cambridge University Press, 1 - 31.

Johnson, H K, H.J Vested, H. Hersbach, J Højstrup and S E Larsen (1999) The coupling between wind and waves in the WAM model. Journ. Atmos. Ocean. Tech, Vol 16, No. 11, 1780 - 1790.

Kaimal, J.C., J.C. Wyngaard, Y. Izumi, and O.R. Coté, 1972: Spectral characteristics of surface-layer turbulence. Quart. J. Roy. Met. Soc., 563--589.

Karagali, I,, A. Pena, M. Badger and C.B. Hasager, Wind characteristics of the North Sea and the Baltic Seas from QuickScatt satellite. Wind Energy. 2012

Lange, B., S.E.Larsen, J. Højstrup and R. Barthelmie, 2004: The influence of thermal effects on the wind speed profile of the coastal marine boundary layer. Boundary-Lay. Meteorol., 112, 587-617

Larsen, S.E. and Jensen, N.O. (1983). Summary and Inter¬pretation of Some Danish Climate Statistics. Risø R 399, 76 pp.

Larsen, S.E., N. E. Tarp-Johansen, S. Frandsen and E. R. Jørgensen, Södra Midsjöbanken Environmental Data-Initial analysis, Risø-I-2505. FP6 Integrated project DOWNVInd- contract 503202

Lettau, H., 1969: Note on aerodynamic roughness-parameter estimation on the basis of roughness-element distribution. J. Appl. Met., 8, 828-832.

Makin, V. K. (2005) A note on the drag of the sea surface at hurricane winds. Boundary Layer Meteorology, 115, 169-175.

Mann, J. , 1998. Wind field simulation, Prob. Engng. Mech. Volume 14, no 4, 269-282,

Melas, D., 1998, The depth of the stably stratified internal boundary layer over the sea. Geophysical Research Letters, 25, No 13, 2261-2264.

Mortensen, N. G. and E.L. Petersen (1997). "Influence of topographical input data on the accuracy of wind flow modeling in complex terrain". 1997 European Wind Energy Conference, Dublin, Ireland.

Olesen, H.R., S.E. Larsen, and J. Højstrup, 1984: Modelling velocity spectra in the lower part of the planetary boundary layer. Boundary-Layer Meteorol., 29, 285--312.

Pena, A., S-E. Gryning and C.B. Hasager, 2008. Measurements and modeling of wind speed profile in the marine atmospheric boundary layer. Boundary Layer Meteorology, 129: 479-495

Pena, A., T. Mikkelsen, S.E. Gryning, C.B. Hasager, A.N. Hahmann, M. Badger, I. Karagali and M. Courtney, Offshore vertical wind shear. Final report NORSEWIND work task 3,1, DTU Wind Energy report 0005 (EN), 2012.

Smedman, A-S., H. Bergström and B. Grisogono, 1997. Evolution of stable internal boundary layers over a cold sea. Journ. Geophys. Research, 102, 1091-1099

Stull, R.B., 1991. An introduction to boundary layer meteorology. Kluwer, 666p

Tennekes, H. and J.L. Lumley (1972) A first course in turbulence. MIT, Cambridge, Mass. 300p.

Troen, I. and E.L. Petersen, 1989: European Wind Atlas. Risø National Laboratory, Roskilde. Denmark.

Wang, H., r. Barthelmie, S.G. pryor, and H-G. Kim (2012) A New Turbulence model for offshore wind standards. Subm. Geophysical Researh.

Zilitinkevich, S.S., 1972: On the determination of the height of the Ekman boundary layer. *Boundary-Layer Meteorol.*, **3**, 141--145.

Zilitinkevich, S.S., 1975: Resistance laws and prediction equations for the depth of the planetary boundary layer. *J. Atmos. Sci.*, **32**, 741--752.

Zilitinkevich, S. , I. Mamarella, A. Baklanov and S. Joffre , 2009. The effect of Stratefication on the aerodynamic roughness length. A, Baklanov et al., eds. Eteorological and Air quality models for urban areas. Springer Berlin.

This Project is part-financed by the South Baltic Programme
and the European Union (European Regional Development Fund).

DTU Wind Energy
Department of Wind Energy

South Baltic
PROGRAMME

This Project is part-financed by the South Baltic Programme and the European Union (European Regional Development Fund).

SOUTH
BALTIC
OFF.E.R